Cutting out the middleman: Calibrating and validating a dynamic vegetation model (ED2-PROSPECT5) using remotely sensed surface reflectance

Alexey N. Shiklomanov[1], Michael C. Dietze[2], Istem Fer[3], Toni Viskari[3], and Shawn P. Serbin[4]

[1]NASA Goddard Space Flight Center, Greenbelt, MD, USA
[2]Department of Earth and Environment, Boston University, Boston, MA, USA
[3]Finnish Meteorological Institute, Helsinki, Finland
[4]Environmental and Climate Sciences Department, Brookhaven National Laboratory, Upton, NY, USA

Correspondence: Dr. Alexey N. Shiklomanov (alexey.shiklomanov@nasa.gov)

Abstract. Ecosystem models are often calibrated and/or validated against derived remote sensing data products, such as MODIS leaf area index. However, these data products are generally based on their own models, whose assumptions may not be compatible with those of the ecosystem model in question, and whose uncertainties are usually not well quantified. Here, we develop an alternative approach whereby we modify an ecosystem model to predict full-range, high spectral resolu-
5 tion surface reflectance, which can then be compared directly against airborne and satellite data. Specifically, we coupled the two-stream representation of canopy radiative transfer in the Ecosystem Demography model (ED2) with a leaf radiative transfer model (PROSPECT 5) and a simple soil reflectance model. We then calibrated this model against reflectance observations from the NASA Airborne VIsible/InfraRed Imaging Spectrometer (AVIRIS) and survey data from 54 temperate forest plots in the northeastern United States. The calibration successfully constrained the posterior distributions of model parameters related
10 to leaf biochemistry and morphology and canopy structure for five plant functional types. The calibrated model was able to accurately reproduce surface reflectance and leaf area index for sites with highly varied forest composition and structure, using a single common set of parameters across all sites. We conclude that having dynamic vegetation models directly predict surface reflectance is a promising avenue for model calibration and validation using remote sensing data.

15 # 1 Introduction

Dynamic vegetation models play a vital role in modern terrestrial ecology, and Earth science more generally. The terrestrial carbon cycle is a major biogeochemical feedback in the global climate system (Heinze et al., 2019), and accurate predictions of terrestrial carbon cycling rely on accurate representations of vegetation dynamics (Pacala and Deutschman, 1995). Vegetation also plays an important role in the water cycle and surface energy balance, with major climate implications (Bo-
20 nan, 2008). In addition, the distribution of tree species, the structure of plant canopies, and many other variables simulated

by dynamic vegetation models are also important predictors of biodiversity, making vegetation models an important tool for conservation (McMahon et al., 2011). Effective calibration and validation of model projections is therefore of broad concern.

Many previous efforts have used various data streams calibrate or constrain dynamic vegetation model parameters and states. Among these data streams, remote sensing is particularly promising due to its consistent measurement methodology and largely uninterrupted global coverage. Data products derived from remote sensing observations have been used to constrain, among others, phenology (Knorr et al., 2010; Viskari et al., 2015), absorbed photosynthetically-active radiation (Peylin et al., 2016; Schürmann et al., 2016), and primary productivity (MacBean et al., 2018). However, there are issues with using derived remote sensing products to calibrate vegetation models. The relationships between remotely sensed surface reflectance and vegetation structure and function are complex and multifaceted. Simple polynomial relationships between spectral indices (e.g., Normalized Difference Vegetation Index, NDVI; Enhanced Vegetation Index, EVI) and vegetation properties (e.g., leaf area index, LAI) are often confounded by other ecosystem characteristics, including soil (Myneni and Williams, 1994) and snow (Zhang et al., 2020), or sensor configuration (Fensholt et al., 2004). More sophisticated approaches for estimating vegetation properties based on physically-based radiative transfer models face issues of equifinality, whereby many different combinations of vegetation and soil properties can ultimately produce the same modeled surface reflectance (Combal et al., 2003; Lewis and Disney, 2007). Meanwhile, the estimating quantities with more indirect relationships to surface reflectance, such as rates of primary productivity, requires a number of assumptions about resource use efficiency and other factors (Running et al., 2004) that can introduce considerable uncertainty and bias into the estimates. Collectively, these issues help explain the large differences in estimates of surface characteristics across different remote sensing instruments (Liu et al., 2018). Robust, pixel-level uncertainty estimates for remote sensing data products would help alleviate some of these concerns, but such estimates are not widely available for most data products.

One way to overcome these limitations of derived remote sensing data products while still leveraging the capabilities of remote sensing is to work with lower-level surface reflectance products. This can be accomplished by coupling dynamic vegetation models with leaf and canopy radiative transfer models that simulate surface reflectance as a function of known surface characteristics (Knorr and Lakshmi, 2001; Nouvellon et al., 2001; Quaife et al., 2008). Such an approach draws on decades of research on simulation of vegetation optical properties given their structural and biochemical characteristics (Dickinson, 1983b; Sellers, 1985; Verhoef, 1984; Lewis and Disney, 2007; Jacquemoud et al., 2009; Pinty et al., 2004; Widlowski et al., 2007, 2015; Hogan et al., 2018) while avoiding the computational and conceptual challenges of inverse parameter estimation in radiative transfer modeling (Combal et al., 2003; Lewis and Disney, 2007). Moreover, the ability to simulate dynamics of surface reflectance in response to changes in ecosystem properties is valuable even independently of its utility for remote sensing data assimilation, as vegetation-induced changes in surface reflectance exert a strong influence on climate (Bonan, 2008; Swann et al., 2010, 2012).

However, externally coupling a vegetation model to a separate canopy radiative transfer model is not always necessary to relate model predictions to surface reflectance, as land surface models have long included their own internal canopy radiative transfer calculations (Dickinson, 1983a; Sellers, 1985). These calculations are necessary to simulate impact of vegetation on surface energy balance (Bonan, 2008) and to accurately model plant function, which is fundamentally driven by light (Hikosaka

and Terashima, 1995; Robakowski et al., 2004; Niinemets, 2016; Keenan and Niinemets, 2016). Canopy radiative transfer plays a particularly important role in the current generation of demographically-enabled dynamic vegetation models, where differences in canopy radiative transfer representations and parametrizations have major impacts on predicted community composition and biogeochemistry (Loew et al., 2014; Fisher et al., 2018; Viskari et al., 2019). To date, assimilation of remotely

60   sensed surface reflectance calculated from a vegetation model's own representation of radiative transfer has been limited to only simple land surface models (e.g., SiPNET; Zobitz et al., 2014) and has not been attempted for more complex demographically-enabled vegetation models.

Our previous work demonstrated that predictions of carbon cycling and community composition by the Ecosystem Demography model, version 2 (ED2; Medvigy et al., 2009) are highly sensitive to changes in parameters related to canopy structure

65   and radiative transfer (Viskari et al., 2019). In this study, we build on this work by calibrating and validating the ED2 model using remotely sensed surface reflectance. First, we couple the internal ED2 canopy radiative transfer model to the PROSPECT 5 leaf radiative transfer model (Feret et al., 2008) and the Hapke soil reflectance model (Verhoef and Bach, 2007) to allow ED2 to predict surface reflectance spectra at 1 nm resolution across the complete visible-shortwave infrared (VSWIR) spectral region (400 to 2500 nm). Second, we jointly calibrate this model at 54 sites in the US Midwest and Northeast where coincident veg-

70   etation survey data and NASA Airborne Visible/Infrared Imaging Spectrometer-Classic (AVIRIS-Classic) surface reflectance observations are available. We hypothesize that, with known stand composition and informative priors on foliar biochemistry, calibration against airborne imaging spectroscopy will significantly constrain model parameters related to canopy structure. Although the scope of our study is limited to the ED2 model, both the underlying size-and-age structure approximation of ED2 as well as many aspects of its canopy radiative transfer (e.g., two-stream approximation, treatment of leaf angles) are common

75   to other land surface models (e.g., FATES; Koven et al., 2020), meaning the insights from this work more broadly applicable in model vegetation modeling.

2   Methods

2.1   ED2 model description

The Ecosystem Demography version 2.2 (ED2) model simulates plot-level vegetation dynamics and biogeochemistry (Moor-

80   croft et al., 2001; Medvigy et al., 2009; Longo et al., 2019a). By grouping individuals of similar size, structure, and composition together into cohorts, ED2 is capable of modeling patch-level competition in a computationally efficient manner. Relevant to this work, ED2 includes a multi-layer canopy radiative transfer model that is a generalization of the two-layer two-stream radiative transfer scheme in CLM 4.5 (Oleson et al., 2013), which in turn is derived from Sellers (1985). A complete description of the model derivation is provided in the supplementary information of Longo et al. (2019a), but for completeness, we provide

85   an abbreviated description below:

Our core spatial unit of analysis is a *patch*—a group of plants with a common disturbance history (time since last disturbance). Each patch contains n *cohorts*—groups of plants of the same plant functional type (PFT) and size class. The full canopy radiation profile in ED2 is defined by a vector $\boldsymbol{X}$ that contains two fluxes—upward ($\boldsymbol{F}_{\mathrm{up},i}$) and downward ($F_{\mathrm{down},i}$)—for each

cohort i, plus a downward flux from the atmosphere ($F_{\text{down,sky}}$) and an upward flux from the ground ($F_{\text{up,ground}}$) surface (total size $2n + 2$):

$$
X = \begin{bmatrix}
F_{\text{up,ground}} \\
F_{\text{down,1}} \\
F_{\text{up,1}} \\
\ldots \\
F_{\text{down},i} \\
F_{\text{up},i} \\
\ldots \\
F_{\text{down},n} \\
F_{\text{up},n} \\
F_{\text{down,sky}}
\end{bmatrix}
\tag{1}
$$

ED2 solves this vector using the following matrix equation:

$$
\mathbf{M} \times X = Y
\tag{2}
$$

where $\mathbf{M}$ is a $(2n + 2) \times (2n + 2)$ coefficient matrix and Y is a $2n + 2$ vector. The full form of Y is as follows:

$$
Y = \begin{bmatrix}
S_0 a_{\text{ground}} \\
S_1 r(\psi)_1 \left[1 - r_0 r_1 (1 - \alpha_0)(1 - \tau_0)(1 - \alpha_1)(1 - \tau_1)\right](1 - \tau(\psi)_1)(1 - \alpha_1) \\
S_1 \left[1 - r_1 r_2 (1 - \alpha_1)(1 - \tau_1)(1 - \alpha_2)(1 - \tau_2)\right](1 - \tau(\psi)_1)(1 - \alpha_1)(1 - r(\psi)_1) \\
\ldots \\
S_i r(\psi)_i \left[i - r_{i-1} r_i (1 - \alpha_{i-1})(1 - \tau_{i-1})(1 - \alpha_i)(1 - \tau_i)\right](1 - \tau(\psi)_i)(1 - \alpha_i) \\
S_i \left[1 - r_i r_{i+1}(1 - \alpha_i)(i - \tau_i)(1 - \alpha_{i+1})(1 - \tau_{i+1})\right](1 - \tau(\psi)_i)(1 - \alpha_i)(1 - r(\psi)_i) \\
\ldots \\
S_n r(\psi)_n \left[1 - r_{n-1} r_n (1 - \alpha_{n-1})(1 - \tau_{n-1})(1 - \alpha_n)(1 - \tau_n)\right](1 - \tau(\psi)_n)(1 - \alpha_n) \\
S_n \left[1 - r_n r_{n+1}(1 - \alpha_n)(1 - \tau_n)(1 - \alpha_{n+1})(1 - \tau_{n+1})\right](1 - \tau(\psi)_n)(1 - \alpha_n)(1 - r(\psi)_n) \\
\text{SW}_{\text{sky}}
\end{bmatrix}
\tag{3}
$$

Here, a_{ground} is the albedo of the ground under the canopy and SW_{sky} is the incident shortwave hemispherical flux from the sky; both are exogenous inputs to the model. S_i is the direct ("beam") radiation at layer i, and is calculated in a loop as follows:

$$
S_i = S_{i+1} \tau(\psi)_i
\tag{4}
$$

with S_{n+1} as the incident direct solar flux at the top of the canopy ($i = n + 1$), an exogenous input.

Other coefficients are backscatter of direct ($r(\psi)_i$, given zenith angle ψ) and diffuse (r_i) radiation, interception of direct ($tau(\psi)_i$) and diffuse (tau_i) radiation, and absorption (α_i). Derivations of these coefficients are given later in this section.

The coefficient matrix $\mathbf{M}$ is a sparse, tridiagonal matrix (i.e., zero elements everywhere except the diagonal and first-order off-diagonal elements); for example, for $n = 3$:

$$
\mathbf{M} =
\begin{bmatrix}
1 & 0 & 0 & 0 & 0 & 0 \\
m_{2,1} & m_{2,2} & m_{2,3} & 0 & 0 & 0 \\
0 & m_{3,2} & m_{3,3} & m_{4,3} & 0 & 0 \\
0 & 0 & m_{4,3} & m_{4,4} & m_{4,5} & 0 \\
0 & 0 & 0 & m_{5,4} & m_{5,5} & m_{5,6} \\
0 & 0 & 0 & 0 & 0 & 1
\end{bmatrix}
\tag{5}
$$

For $i = 1, 2, 3 \ldots n$ where n is the number of cohorts, the m terms are defined as follows:

$$
m_{1,1} = 1
$$
$$
m_{2i,2i-1} = -\left[\tau_i + (1 - \tau_i)(1 - \alpha_i)(1 - r_i)\right]
$$
$$
m_{2i,2i} = -r_{i-1}\left[\tau_i + (1 - \tau_i)(1 - \alpha_i)(1 - r_i)\right](1 - \alpha_{i-1})(1 - \tau_{i-1})
$$
$$
m_{2i,2i+1} = 1 - r_{i-1}r_i(1 - \alpha_{i-1})(1 - \tau_{i-1})(1 - \alpha_i)(1 - \tau_i)
$$
$$
m_{2i+1,2i} = 1 - r_i r_{i+1}(1 - \alpha_i)(1 - \tau_i)(1 - \alpha_{i+1})(1 - \tau_{i+1})
$$
$$
m_{2i+1,2i+1} = -r_{i+1}\left[\tau_i + (1 - \tau_i)(1 - \alpha_i)(1 - r_i)\right](1 - \alpha_{i+1})(1 - \tau_{i+1})
$$
$$
m_{2i+1,2i+2} = -\left[\tau_i + (1 - \tau_i)(1 - \alpha_i)(1 - r_i)\right]
$$
$$
m_{2n+2,2n+2} = 1
\tag{6}
$$

Canopy optical property coefficients are derived as follows:

Following Oleson et al. (2013), forward- (ν) and backscattering (ω) of canopy elements (leaves or stems) are defined as a function of those elements' reflectance (R) and transmittance (T; wood transmittance is assumed to be zero). (We use index p to refer to PFT and $p(i)$ to refer to the PFT of cohort i).

$$
\nu_{i,\text{leaf}} = R_{p(i),\text{leaf}} + T_{p(i),\text{leaf}}
$$
$$
\nu_{i,\text{wood}} = R_{p(i),\text{wood}}
$$

$$
\tag{7}
$$

$$\omega_{i,\mathrm{leaf}} = \frac{R_{p(i),\mathrm{leaf}} + T_{p(i),\mathrm{leaf}} + \frac{1}{4}(R_{p(i),\mathrm{leaf}} - T_{p(i),\mathrm{leaf}})(1 - \chi_{p(i)})^2}{2(R_{p(i),\mathrm{leaf}} + T_{p(i),\mathrm{leaf}})}$$

$$\omega_{i,\mathrm{wood}} = \frac{R_{p(i),\mathrm{wood}} + \frac{1}{4}(R_{p(i),\mathrm{wood}})(1 - \chi_{p(i)})^2}{2R_{p(i),\mathrm{wood}}} \tag{8}$$

where χ is the *leaf orientation factor* parameter, defined such that -1 is perfectly vertical leaves, 1 is perfectly horizontal leaves, and 0 is randomly distributed leaf angles. Both of these quantities are calculated independently for leaves and wood, and then averaged based on the relative effective area of leaves (L_i) and wood (W_i) within a canopy layer.

$$\nu_i = \nu_{i,\mathrm{leaf}} \frac{L_i}{L_i + W_i} + \nu_{i,\mathrm{wood}}(1 - \frac{L_i}{L_i + W_i}) \tag{9}$$

$$\omega_i = \omega_{i,\mathrm{leaf}} \frac{L_i}{L_i + W_i} + \omega_{\mathrm{wood}}(1 - \frac{L_i}{L_i + W_i}) \tag{10}$$

To account for non-uniform distribution of leaves within a canopy, ED2 has a PFT-specific *clumping factor* (q) parameter that serves as a scaling factor on leaf area index. Therefore the effective leaf area index (L) is related to the true leaf area index (LAI) by:

$$L_i = \mathrm{LAI}_i \times q_{p(i)} \tag{11}$$

The leaf area of a cohort (LAI_i) is calculated as a function of leaf biomass ($B_{\mathrm{leaf},i}$, kgC plant^{-1}), specific leaf area (SLA$_p$, m^2 kgC^{-1}), and stem density (n_{plant}, plants m^{-2}):

$$\mathrm{LAI}_i = n_{\mathrm{plant},i} B_{\mathrm{leaf},i} \mathrm{SLA}_{p(i)} \tag{12}$$

In turn, $B_{\mathrm{leaf},i}$ is calculated from cohort diameter at breast height (DBH$_i$, cm) according to the following allometric equations:

$$B_{\mathrm{leaf},i} = \mathrm{b1Bl}_{p(i)} \mathrm{DBH}_i^{\mathrm{b2Bl}_{p(i)}} \tag{13}$$

where $\mathrm{b1Bl}_{p(i)}$ and $\mathrm{b2Bl}_{p(i)}$ are PFT-specific parameters. The wood area of a cohort (WAI$_i$) is calculated directly from DBH according to a similar allometric equation:

$$\mathrm{WAI}_i = n_{\mathrm{plant},i} \mathrm{b1Bw}_{p(i)} \mathrm{DBH}_i^{\mathrm{b2Bw}_{p(i)}} \tag{14}$$

135   where $\mathrm{b1Bw}_{p(i)}$ and $\mathrm{b2Bw}_{p(i)}$ are PFT-specific parameters.

The directional extinction coefficient ($K(\psi)_p$)—closely related to the inverse optical depth for direct radiation ($\mu_{0,p}$)—can be expressed as:

$$K(\psi)_p = \mu_{0,p}^{-1} = \frac{G(\psi)_p}{\cos(\psi)} \tag{15}$$

where $G(\psi)_p$ describes the mean projection per unit leaf area (or "relative projected leaf area") in direction ψ.

140   As in CLM 4.5 (Oleson et al., 2013) and Sellers (1985), the leaf angle distribution function and parameterization used in ED2 is based on Goudriaan (1977):

$$G(\psi)_p = \phi_{1,p} + \phi_{2,p} \cos(\psi) \tag{16}$$

$$\phi_{1,p} = 0.5 - 0.633\chi_p - 0.33\chi_p^2 \tag{17}$$

$$\phi_{2,p} = 0.877(1 - 2\phi_{1,p}) \tag{18}$$

145   Coefficients $\phi_{1,p}$ and $\phi_{2,p}$ are also used to define the inverse optical depth for diffuse radiation per unit plant area ($\bar{\mu}_p$) (subscript p is omitted from the next three equations for convenience):

$$\bar{\mu} = \frac{1}{\phi_2}\left(1 - \frac{\phi_1}{\phi_2}\ln\left(1 + \frac{\phi_2}{\phi_1}\right)\right) \tag{19}$$

The beam backscatter (or "upscatter") coefficient for direct radiation, β_0, is defined as:

$$\beta_0 = a_s(\psi)\frac{1 + \bar{\mu}K(\psi)}{\bar{\mu}_p K(\psi)_p} \tag{20}$$

150   where $a_s(\psi)$ is the single scattering albedo coefficient, defined as (subscript p dropped for simplicity):

$$a_s(\psi) = \frac{1}{2}\frac{G(\psi)}{\phi_2\cos\psi + G(\psi)}\left(1 - \frac{\phi_1\cos\psi}{\cos\psi + G(\psi)}\ln\left(\frac{\phi_1\cos\psi + \phi_2\cos\psi + G(\psi)}{\phi_1\cos\psi}\right)\right) \tag{21}$$

(For simplicity, a_s here is equivalent to $\frac{a_s}{\omega}$ in Oleson et al. (2013) equation 3.15, where ω is the leaf backscatter.)

The transmissivity of a layer to direct radiation for solar zenith angle ψ ($\tau(\psi)_i$) is given by

$$\tau(\psi)_i = \exp(-K(\psi)_{p(i)}\mathrm{TAI}_i) \tag{22}$$

155   where TAI_i is the total plant area index (sum of effective leaf area index, L_i, and wood area index, W_i).

2.2 ED2-PROSPECT coupling

By default, ED2 performs canopy shortwave radiative transfer calculations for two broad spectral regions: visible (400–700 nm) and near-infrared (700–2500 nm). For each of these regions, ED2 has user-defined prescribed leaf and wood reflectance and transmittance for each PFT, and calculates soil reflectance as the average of constant wet and dry soil reflectance values weighted by the relative soil moisture (0 = fully dry, 1 = fully wet). In this study, we modified ED2 to perform the same canopy radiative transfer calculations but in 1 nm increments across the range 400–2500 nm. We then simulated leaf reflectance and transmittance using the PROSPECT 5 leaf RTM, which has the following five parameters: Effective number of leaf mesophyll layers (N, unitless, >= 1), total chlorophyll content (Cab, µg cm^{-2}), total carotenoid content (Car, µg cm^{-2}), water content (Cw, g cm^{-2}), and dry matter content (Cm, g cm^{-2}) (Feret et al., 2008). For wood reflectance, we used a single representative spectrum—the mean of all wood spectra from Asner (1998), resampled to 1 nm resolution—for all PFTs. For soil reflectance, we used the simple Hapke soil submodel used in the Soil-Leaf-Canopy RTM (Verhoef and Bach, 2007), whereby soil reflectance is the average of prescribed wet and dry soil reflectance spectra weighted by a relative soil moisture parameter (ϱ_{soil}, unitless, 0–1). The final coupled PROSPECT-ED2 canopy radiative transfer model (hereafter known as "EDR") has 12 parameters for each PFT— 5 parameters for PROSPECT, specific leaf area, two parameters each for the leaf and wood allometries, and clumping and orientation factors—and one site-specific parameter—the relative soil moisture (Table 1).

2.3 Site and data description

For model calibration, we selected 54 sites from the NASA Forest Functional Types (FFT) field campaign that contained plot-level inventory data (stem density, species identity, and diameter at breast height, DBH) coincident with observations of the NASA Airborne Visible/Infrared Imaging Spectrometer-Classic (AVIRIS-Classic). These sites are located in the United States Upper Midwest, northern New York, and western Maryland, and include stands dominated by either evergreen or deciduous trees and spanning a wide range of structures, from dense groups of saplings to sparse groups of large trees (Figure 1). We grouped the tree species in these sites into five different PFTs as defined by ED2: Early successional hardwood, northern mid-successional hardwood, late successional hardwood, northern pine, and late successional conifer. The mappings of tree species onto these PFTs are provided as a CSV-formatted table in the file `inst/pfts-species.csv` in the source code repository for this project (see Code and Data Availability section).

AVIRIS-Classic measures directional surface reflectance from 365 to 2500 nm at approximately 10 nm increments. However, because of unrealistic values in the shortwave infrared spectral region (>1300 nm) in the AVIRIS observations (likely caused by faulty atmospheric correction), we only used observations from 400 to 1300 nm for model calibration and validation. Following Shiklomanov et al. (2016), we used the relative spectral response functions of AVIRIS-Classic to relate the 1 nm EDR predictions to the 10 nm AVIRIS-Classic measurements.
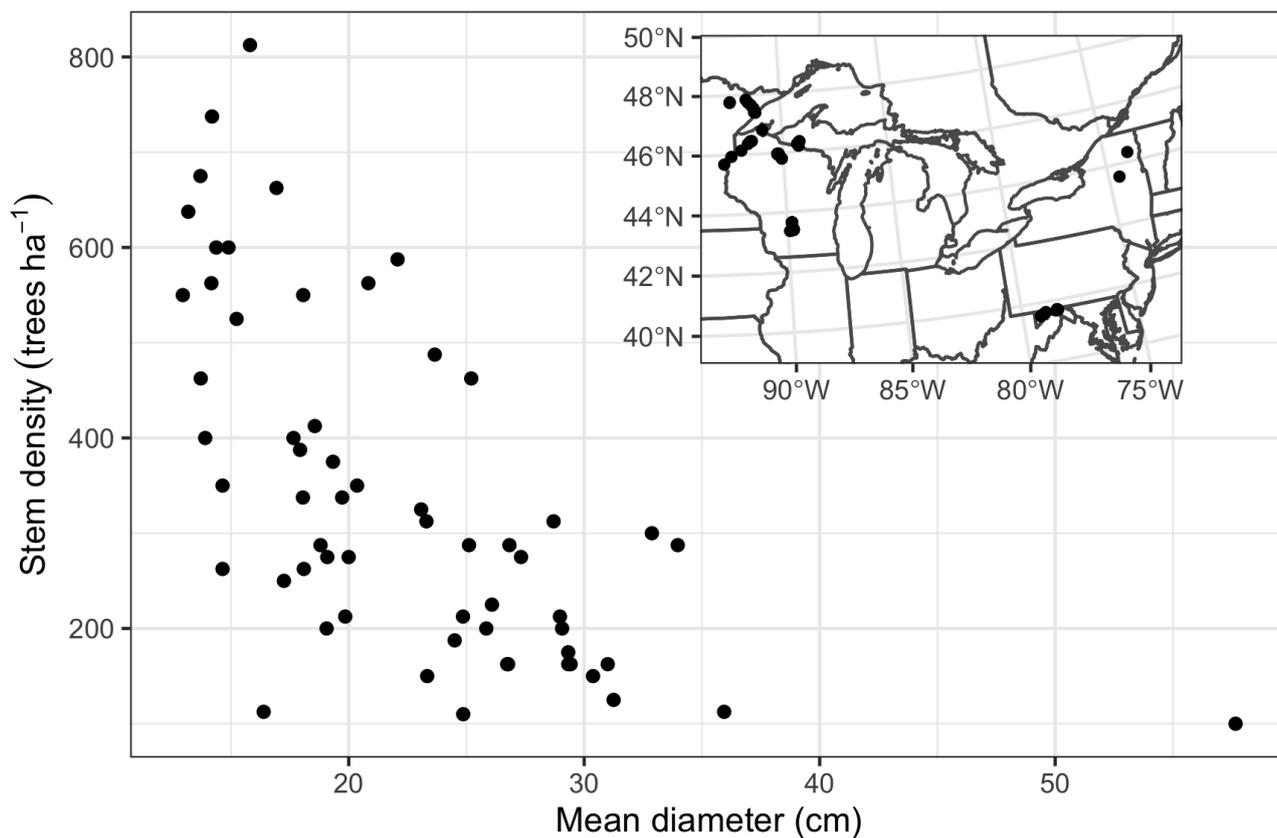
Figure 1. Sites selected for analysis, in "stand structure" (*main figure*) and geographic (*inset*) space.

2.4 Model calibration

To estimate EDR parameters from AVIRIS observations, we used a Bayesian approach that builds on our previous work at the leaf scale (Shiklomanov et al., 2016). For a parameter vector Θ and matrix of observations $\mathbf{X}$, the typical form of Bayes' rule is given by:

$$\underbrace{P(\mathbf{\Theta}|\mathbf{X})}_{\text{Posterior}} \sim \underbrace{P(\mathbf{X}|\mathbf{\Theta})}_{\text{Likelihood}} \underbrace{P(\mathbf{\Theta})}_{\text{Prior}} \tag{23}$$

190

Rather than performing a separate calibration at each site, we performed a single joint calibration across all sites. Therefore, our overall likelihood ($P(\mathbf{X}|\mathbf{\Theta})$) was the product of the likelihood at each site ($P(\mathbf{X}_s|\mathbf{\Theta})$, for site s):

$$P(\mathbf{X}|\mathbf{\Theta}) = \prod_s P(\mathbf{X}_s|\mathbf{\Theta}) \tag{24}$$

The likelihood at each site s is based on how well EDR predicted surface reflectance ($R_{\mathrm{pred},s}$) matches that site's observed
195 AVIRIS surface reflectance ($\mathbf{X}_s$) given the known forest composition at that site (comp_s) and the current estimate of the overall parameter vector. Similar to Shiklomanov et al. (2016), we assumed a normally-distributed residual error between predicted and observed reflectance. However, to account for the large differences in the range of feasible reflectance values in different wavelength regions (for vegetation, reflectance in the 400-700 nm range is typically much lower than in the 700-1400 nm range), we used a heteroskedastic error model where the residual variance was a linear function of the predicted reflectance
200 (with slope m and intercept b). In addition, to mitigate sampling issues related to EDR's saturating response to increasing total LAI, we added an additional term to our likelihood that assigns a fixed lognormal probability distribution (with parameters 1 and 0.5, respectively) to the EDR predicted LAI for a given site ($\mathrm{LAI}_{\mathrm{pred},s}$). The expression for the site-specific likelihood is therefore:

$$R_{\mathrm{pred},s}, \mathrm{LAI}_{\mathrm{pred},s} = \mathrm{EDR}(\mathbf{\Theta}|\mathrm{comp}_s) \tag{25}$$

205 $$P(\mathbf{X}_s|\mathbf{\Theta}) = \mathrm{Normal}(\mathbf{X}_s|R_{\mathrm{pred},s}, mR_{\mathrm{pred},s} + b) \, \mathrm{LogNormal}(\mathrm{LAI}_{\mathrm{pred},s}|1, 0.5) \tag{26}$$

Therefore, our parameter vector $\mathbf{\Theta}$ consists of the following (summarized in Table 1): 10 EDR parameters per PFT—5 parameters for the PROSPECT 5 model (*N*, *Cab*, *Car*, *Cw*, *Cm*) and 5 EDR parameters related to canopy structure (q, χ, SLA, b1Bl, b1Bw)—, 1 parameter per site (relative soil moisture, $\varrho_{\mathrm{soil},s}$), and the residual slope (m) and intercept (b). (With 5 PFTs and 54 sites, this means that $\mathbf{\Theta}$ has length $(10 \times 5) + 54 + 2 = 106$).

210 For priors on the PROSPECT 5 parameters and SLA, we performed a hierarchical multivariate analysis (Shiklomanov et al., 2020) on PROSPECT 5 parameters and direct SLA measurements from (Shiklomanov, 2018, Chapter 3). For priors on the leaf biomass allometry parameters, we fit a multivariate normal distribution to allometry coefficients from Jenkins et al. (2003, 2004) using the `PEcAn.allometry` package (https://github.com/pecanproject/pecan/tree/develop/modules/allometry). For the clumping factor, we used a uniform prior across its full range (0 to 1), and for the leaf orientation factor, we used a weakly
215 informative beta distribution re-scaled to the range $(-1, 1)$ and centered on 0.5 (Table 1).

To alleviate issues with strong collinearity between the allometry parameters and the specific leaf area, we fixed the allometry exponent parameters (b2Bl and b2Bw) to their prior means for each PFT. Doing so dramatically improved the stability of the inversion algorithm and the accuracy of the results.

We fit this model using the Differential Evolution with Snooker Update ("DEzs") Markov-Chain Monte Carlo (MCMC)
220 sampling algorithm (ter Braak and Vrugt, 2008) as implemented in the R package `BayesianTools` (Hartig et al., 2019). We

Table 1. EDR parameters and prior distributions

Type	Name	Description	Unit	Prior
Leaf RTM parameters	N	Effective number of leaf mesophyll layers	unitless	$\text{MvNormal}(\boldsymbol{\mu}, \boldsymbol{\Sigma})$[1]
(1 per PFT)	Cab	Total leaf chlorophyll content	µg cm^{-2}	$\text{MvNormal}(\boldsymbol{\mu}, \boldsymbol{\Sigma})$[1]
	Car	Total leaf carotenoid content	µg cm^{-2}	$\text{MvNormal}(\boldsymbol{\mu}, \boldsymbol{\Sigma})$[1]
	Cw	Leaf water content	g cm^{-2}	$\text{MvNormal}(\boldsymbol{\mu}, \boldsymbol{\Sigma})$[1]
	Cm	Leaf dry matter content	g cm^{-2}	$\text{MvNormal}(\boldsymbol{\mu}, \boldsymbol{\Sigma})$[1]
Canopy RTM parameters	SLA	Specific leaf area	kg m^{-2}	$\text{MvNormal}(\boldsymbol{\mu}, \boldsymbol{\Sigma})$[1]
(1 per PFT)	q	Canopy clumping factor	unitless	$\text{Uniform}(0,1)$
	χ	Leaf orientation factor	unitless	$2 \times \text{Beta}(18,12) - 1$
	b1Bl	Leaf biomass allometry base	unitless	$\text{LogNormal}(m_l, s_l)$[2]
	b1Bw	Wood biomass allometry base	unitless	$\text{LogNormal}(m_w, s_w)$[2]
Other parameters	$\varrho_{\text{soil},s}$	Relative soil moisture content at site s	unitless	$\text{Uniform}(0,1)$
	a	Residual slope	unitless	$\text{Exponential}(1)$
	b	Residual intercept	unitless	$\text{Exponential}(10)$

[1] PFT-specific multivariate normal distribution fit to PROSPECT parameters and SLA from Shiklomanov (2018), chapter 3.

[2] PFT-specific results from Bayesian fits of allometric equations to allometry data from Jenkins et al. (2003, 2004) using the `PEcAn.allometry` package.

ran the algorithm using 8 independent chains for as many iterations as required to achieve convergence, assessed according to a Gelman-Rubin Potential Scale Reduction Factor (PSRF) diagnostic value of less than 1.1 for all parameters (Gelman and Rubin, 1992).

2.5 Analysis

225 To assess the extent to which AVIRIS-Classic observations were able to constrain parameter estimates, we compared the prior and posterior distributions for all parameters. To evaluate the performance of the calibrated model, we compared the posterior credible and predicted 95% intervals of EDR-predicted spectra against the AVIRIS observations at each site. We also compared the EDR-predicted LAI against field observations at each site. To evaluate goodness-of-fit and additive and multiplicative biases, we used an ordinary least squares regression of mean observed vs. posterior mean predicted LAI.

230 ## 3 Results

Model calibration improved the precision of most PFT-specific parameter estimates, including parameters whose prior distributions were informative (Figure 2). For leaf traits, PFT rankings of the posterior estimates largely followed the relative positions of the priors. The effective number of leaf layers (PROSPECT N parameter) was higher for needleleaved than broadleaved PFTs, with the highest value for northern pine and the lowest value for mid hardwood. Estimated total chlorophyll contents
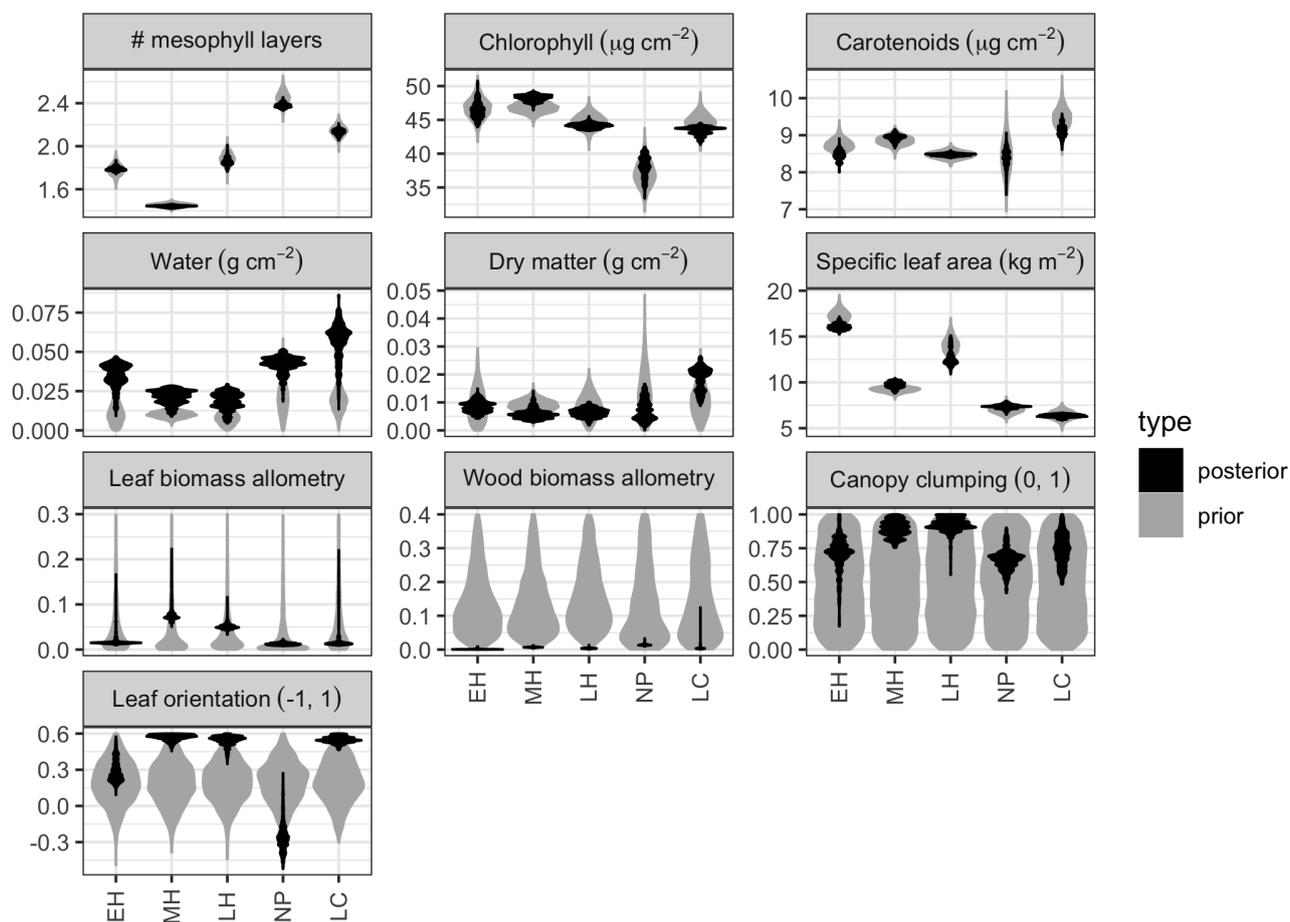
Figure 2. Marginal prior (pre-calibration; grey) and posterior (post-calibration; black) distributions of PFT-specific parameters related to leaf biochemistry and canopy structure. Distributions are shown as violin plots (rotated and mirrored kernel density plots). PFTs are abbreviated as follows: EH:Early Hardwood; MH:North Mid Hardwood; LH:Late Hardwood; NP:Northern Pine; LC:Late conifer
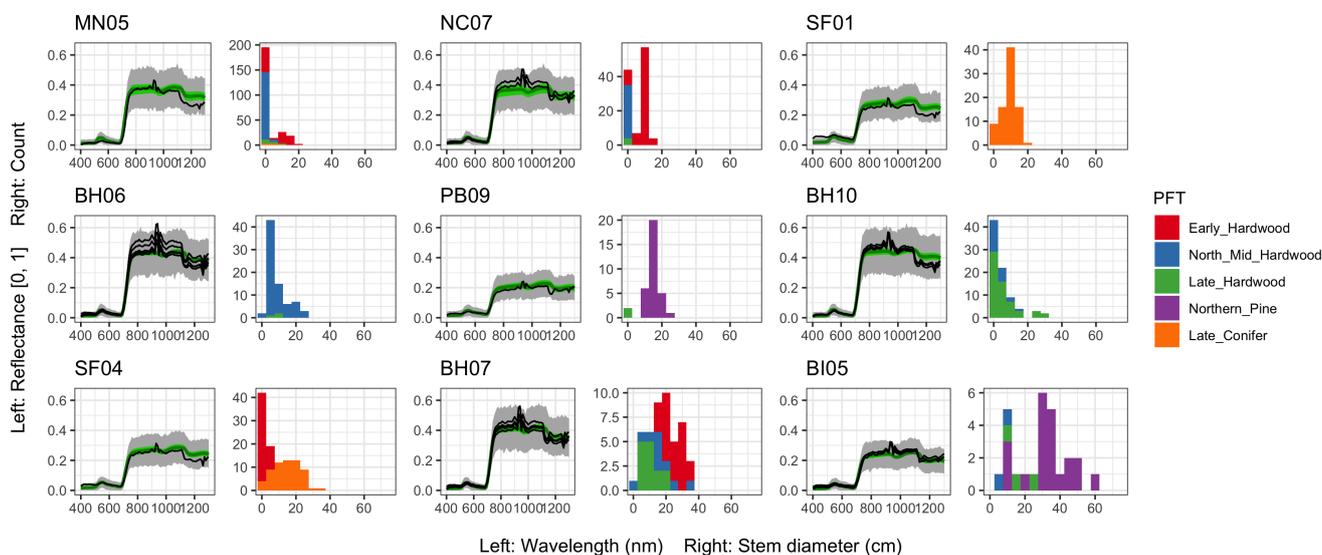
Figure 3. (*Left*) Comparison between AVIRIS observed (black) and EDR predicted (mean prediction in green, 95% posterior predictive interval in gray) surface reflectance for a sample of sites used in the calibration. (*Right*) Histogram of stem diameter at breast height (DBH) by plant functional type (PFT) at the corresponding site.

(*Cab*) were similar across all PFTs, with the highest values for early and mid Hardwood followed closely by late hardwood and late conifer, and the lowest values for northern pine. Estimates of leaf total carotenoid (*Car*), water (*Cw*), and dry matter contents (*Cm*) had distributions that overlapped for all PFTs, though the central tendency of late conifer was slightly higher than other PFTs for all three traits. Finally, estimated specific leaf area (SLA) was highest in early hardwood, followed by late hardwood and mid hardwood, and was comparably low for northern pine and late conifer.

Compared to leaf traits, canopy structural traits had less informative (and PFT-agnostic) priors and were more constrained by the calibration. Although the estimated parameter distributions were still mutually overlapping in most cases, the constraint did suggest differences between PFTs for some parameters. For example, leaf orientation factors and, to a lesser extent, canopy clumping factors and leaf biomass allometry parameters (*b1Bl*) were higher for mid- and late-successional broadleaved PFTs than other PFTs. Meanwhile, northern pine had the lowest leaf biomass allometry parameters and clumping and orient factors, and the highest wood biomass allometry parameter (*b1Bw*). Calibration provided only limited constraint on site-specific soil optical properties, with posterior estimates that were typically almost as wide as the uninformative prior distributions for all but a few specific sites (Figure A1).

The accuracy and precision of EDR simulated spectra relative to AVIRIS observations varied across sites (Figures 3, 4, and A2). The largest differences between observed and predicted reflectance were in the near-infrared region, particularly from 775 to 1100 nm, while predictions in the visible range agreed well with observations in all but a few cases. That said, the EDR predictive interval overlapped observations in all but a few individual cases (Figure A2), suggesting that our estimates of
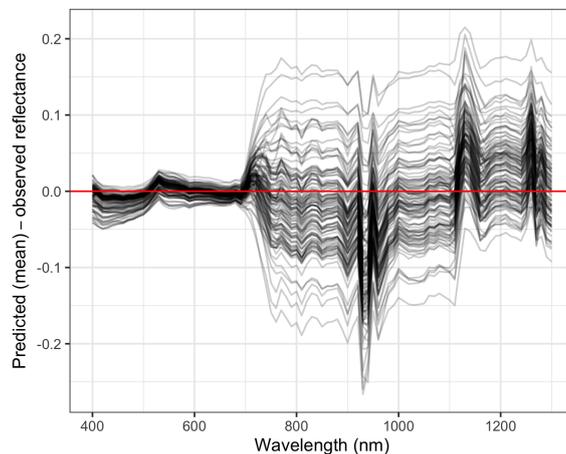
Figure 4. Difference between AVIRIS observed and EDR predicted (mean) site surface reflectance. One line per site and observation is shown (some sites had multiple observations).
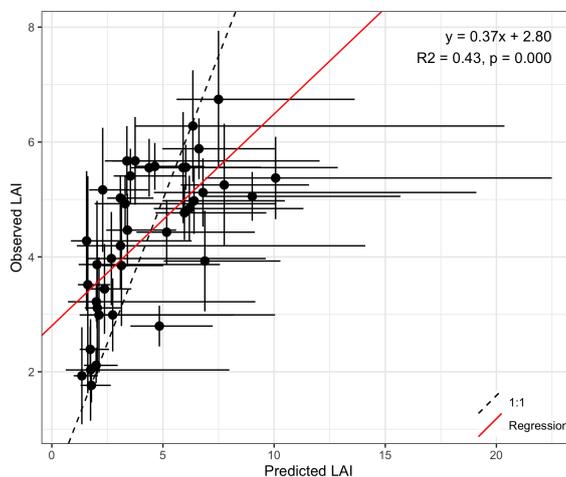
Figure 5. EDR predictions of leaf area index (LAI) compared to observed values.

model uncertainty are realistic. We did not observe any consistent patterns in mismatch between observed and EDR predicted reflectance with respect to tree size, stem density, or composition (Figures A3–A13).

Leaf area index predicted from calibrated EDR parameters captured 43% of the variability in the observations (Figure 5).
255 The observed vs. predicted line had a slope of 0.37 and an intercept of 2.80, indicating that EDR calibration underpredicted LAI on average but overexagerrated across-site LAI variability.

4   Discussion

Calibrating and validating vegetation models using optical remote sensing data typically involves derived data products (e.g., MODIS GPP) that rely on their own models; in other words, "bringing the observations closer to the models". In this study, we presented an alternative approach whereby we bring the models closer to the observations by training a vegetation model to simulate full-range hyperspectral surface reflectance as observed by optical remote sensing instruments. We then demonstrated how this approach could be used to calibrate the model against airborne imaging spectroscopy data from AVIRIS-Classic. We found that such calibration reduced uncertainties in parameters related to leaf biochemistry and canopy structure, even for parameters with well-informed priors (Figure 2). Moreover, we found that that the calibrated model was able to reproduce observed surface reflectance (Figures 3 and 4) and leaf area index (Figure 5) reasonably well across large number of structurally, compositionally, and geographically diverse sites (Figure 1).

Compared to previous similar efforts that have coupled vegetation models to external canopy radiative transfer models (Knorr and Lakshmi, 2001; Nouvellon et al., 2001; Quaife et al., 2008), our work is novel because it uses a canopy radiative transfer formulation that *already exists inside the model itself*. This reduces the number of new assumptions and variables we have to introduce and increases the extent to which constraint on canopy radiative transfer parameters propagates to other related processes in the model. For example, to couple the Geometric Optic Radiative Transfer (GORT) model to the Data Assimilation Linked Ecosystem Carbon (DALEC) model, Quaife et al. (2008) had to assume a relationship between the GORT-predicted foliage area volume density and DALEC-predicted foliar biomass, which required introducing an additional fixed parameter (grams of leaf carbon per leaf area) present in neither model. More importantly, in such a coupling, the only way that observed reflectance constrains the model is through the foliar biomass, and additional information from the reflectance on canopy structure is confined to the GORT parameters. By contrast, in our approach, parameters and states in the shortwave canopy radiative transfer submodel also influence other model processes, including thermal radiative transfer, micrometeorology, and competition (Longo et al., 2019b), with profound consequences for model predictions of ecosystem fluxes and composition (Viskari et al., 2019).

The canopy radiative transfer model in ED2 is derived from the two-stream model of Sellers (1985) and adapted to a multi-level canopy. Similar versions of this two-stream formulation are present in other land surface models, including CLM (Oleson et al., 2013), SiB (Baker et al., 2008), Noah (Niu et al., 2011), tRIBS-VEGGIE (Ivanov et al., 2008), IMOGEN (Huntingford et al., 2008), and JULES (Best et al., 2011). Although the exact parameterization and implementation differs across these models, the similarity of the underlying conceptual framework means that our approach should be directly transferable to all of these models as well.

One limitation of the two-stream canopy radiative transfer approach in the context of remote sensing is the absence of any angular information in the output. More precisely, the quantity simulated by EDR is the bi-hemispherical reflectance (BHR), whereas the atmospherically-corrected AVIRIS-Classic quantity is closest to the hemispherical-directional reflectance factor (HDRF) (Schaepman-Strub et al., 2006, *sensu*). Under specific sun-sensor geometries and atmospheric and illumination conditions, canopy reflectance can have a significant angular dependence, especially in sparse or structurally complex canopies (e.g.,

"hot spot effect"; Maignan et al., 2004; Schaepman-Strub et al., 2006). However, in simulations of black spruce canopy BHR and HDRF under different conditions, Schaepman-Strub et al. (2006) find differences of no more than 2% between these quantities in the 650–670 nm region, which are smaller than the width of the predictive uncertainty intervals in our results for the same wavelengths (Figure 3). Moreover, the lower altitude and narrow field-of-view of the AVIRIS-Classic instrument used in this study mean that all observer zenith angles are effectively nadir or very close, Finally, multiple versions of the two-stream approximation developed over the last 20 years have been validated against reflectance from more complex 3D ray-tracing simulations and remotely sensed observations, and none have identified treatment of angular effects as the primary source of uncertainty (Hogan et al., 2018; Yuan et al., 2017; Pinty et al., 2004). We therefore conclude that additional computational and conceptual challenges (as well as parameter uncertainties) associated with treatment of angular effects in similar models are unwarranted.

A related issue is the missing or simplistic treatment of two- and three-dimensional heterogeneity in canopy structure in EDR. For one, the treatment of leaves as infinitely small elements randomly distributed through the canopy space—a common feature of all two-stream approximations—neglects complex realities of the canopy light environment such as gaps and self-shading. In EDR, self-shading is handled via the clumping factor parameter, which functions as a scalar correction on the leaf area index (Equation 11). A key feature of EDR design is its representation of multiple co-existing plant cohorts competing for light within a single patch; however, horizontal heterogeneity and competition between these cohorts is ignored. Improved representation of lateral energy transfer can improve the accuracy of simulations of the canopy light environment, and recent theoretical advances show that this can be accomplished without a significant loss in computational performance (Hogan et al., 2018). Treatment of horizontal competition also plays an important role in the outcomes of competition for light between different plants (Fisher et al., 2018). A useful avenue for development and parameterization of these models is comparison to more sophisticated and realistic three-dimensional representations of radiative transfer (e.g. Widlowski et al., 2007), which are themselves too computationally demanding to be coupled to ecosystem models, but from which empirical distributions and response functions could be derived and against which the behavior of simpler models could be evaluated.

5 Conclusions

Remote sensing observations are unrivaled in their spatial completeness and extent, notably extending to regions like the tropics and high latitudes that are relatively undersampled but have a disproportionate impact on the global climate system (Schimel et al., 2015) and/or global biodiversity (Jetz et al., 2016). At the same time, satellite time series provide multidecadal records with relatively high temporal frequency, which have tremendous utility for calibrating model projections of past ecological dynamics (Kennedy et al., 2014; Pasquarella et al., 2016). Used in combination with other emerging data sources, including global trait databases and eddy covariance measurements, remote sensing can be a transformative force in ecosystem ecology.

In this paper, we showed that using a vegetation model to directly simulate surface reflectance is a promising approach for calibrating and validating models against remotely sensed observations. To do this, we modified the ED2 dynamic vegetation model to predict full-range hyperspectral surface reflectance and then calibrated this modified model against airborne imaging

spectroscopy data. The calibration successfully constrained the distributions of model parameters related to canopy structure

325 and leaf biogeochemistry for five plant functional types for five plant functional types characteristic of temperate forests of the northeastern United States. The calibrated model was able to accurately reproduce surface reflectance and leaf area index for sites with highly varied forest composition and structure, using a single common set of parameters (i.e., not site-specific parameters). Although our study focused only on the ED2 model, the basic structure and assumptions of the ED2 canopy radiative transfer scheme are shared by many other vegetation models, so we expect that our approach has high transferability

330 within the vegetation modeling community.

Code and data availability. All of the code and data required to reproduce this study are publicly available via an Open Science Framework (OSF) project, located at https://osf.io/b6umf/.

Appendix A: Supplementary figures
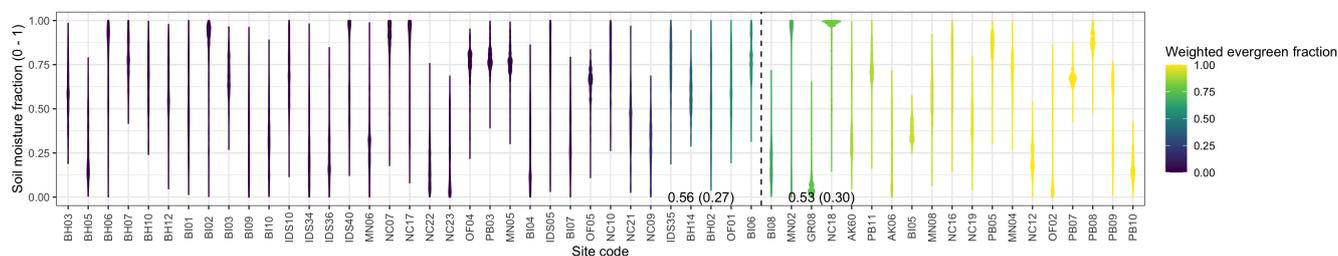
Figure A1. Site-specific relative soil moisture (0 = dry, 1 = wet) posterior estimates. Sites are sorted in order of increasing weighted evergreen fraction.
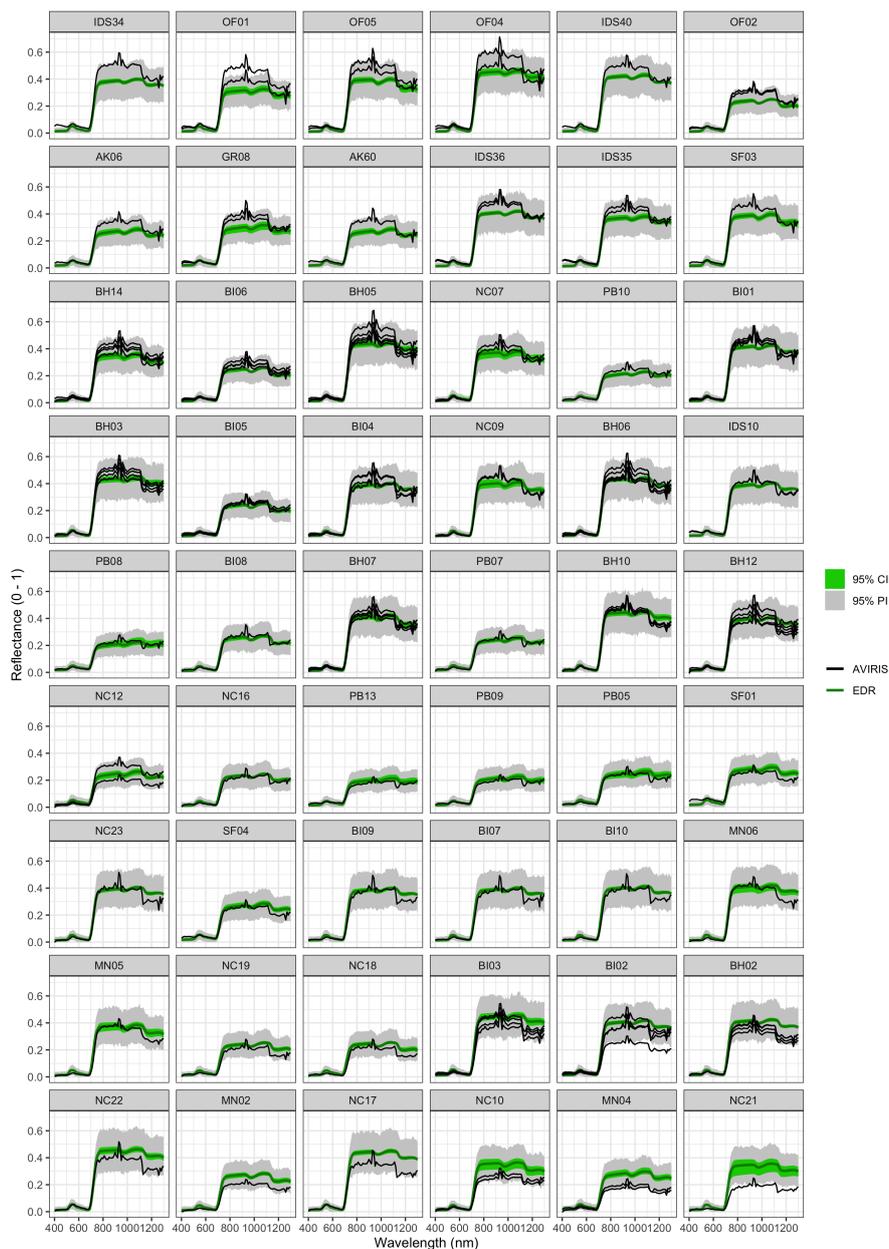
Figure A2. Comparison between AVIRIS observed (black) and surface reflectance for each site used in the calibration. Sites are sorted in order of decreasing mean difference between observed and EDR predicted reflectance (largest underestimates first, largest overestimates last).
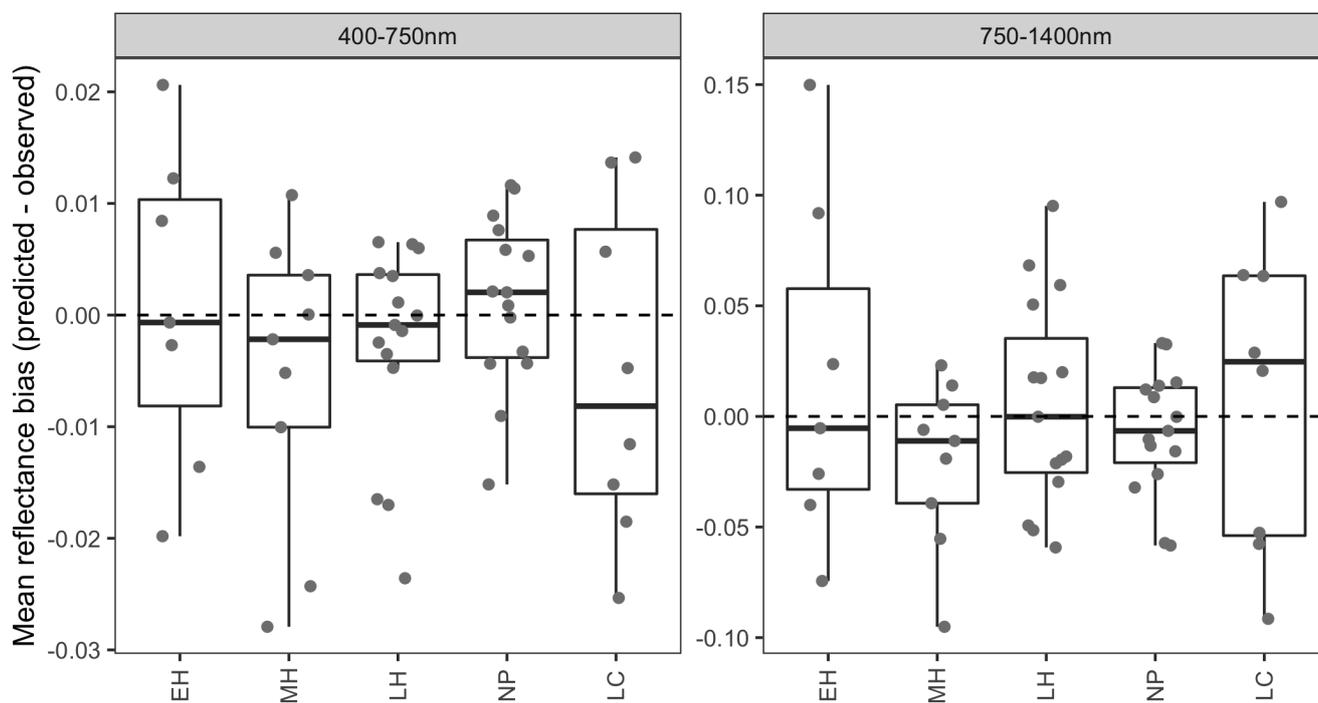
Figure A3. Mean reflectance bias (EDR predicted - observed) for each by spectral region and dominant plant functional type (PFT). PFTs are abbreviated as follows: EH:Early Hardwood; MH:North Mid Hardwood; LH:Late Hardwood; NP:Northern Pine; LC:Late conifer
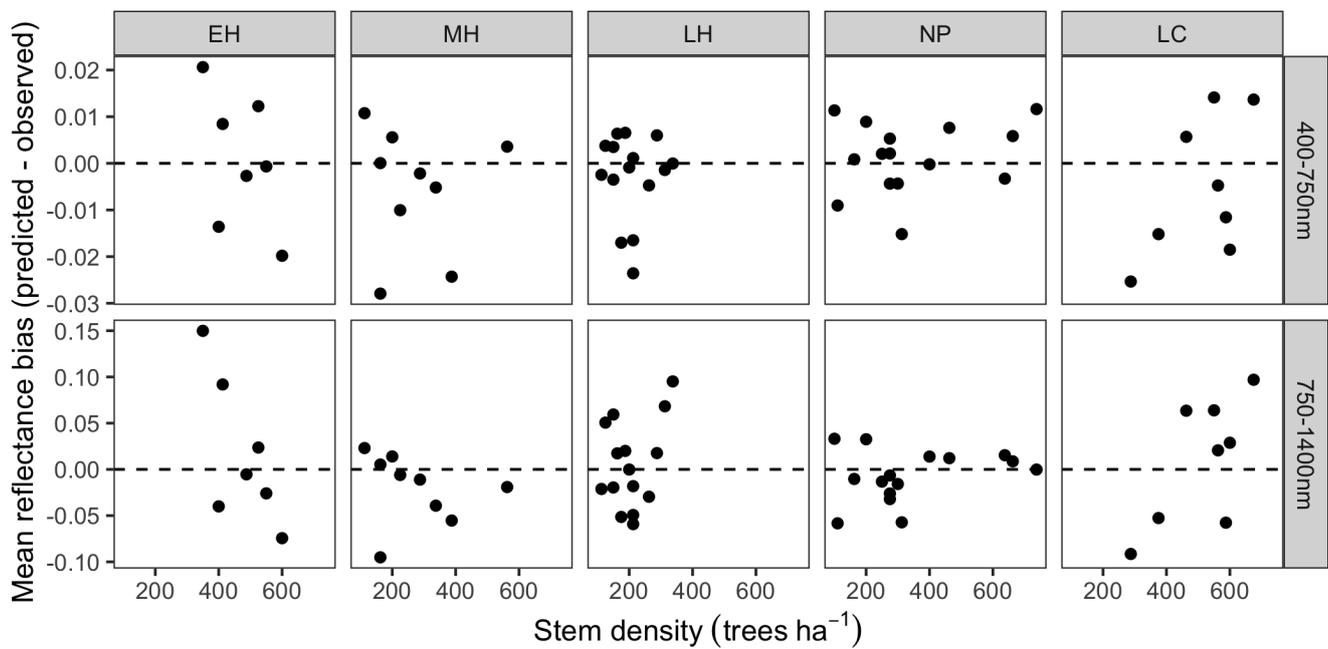
Figure A4. Mean reflectance bias (EDR predicted - observed) for each by spectral region and dominant plant functional type (PFT) as a function of site stem density. PFTs are abbreviated as follows: EH:Early Hardwood; MH:North Mid Hardwood; LH:Late Hardwood; NP:Northern Pine; LC:Late conifer
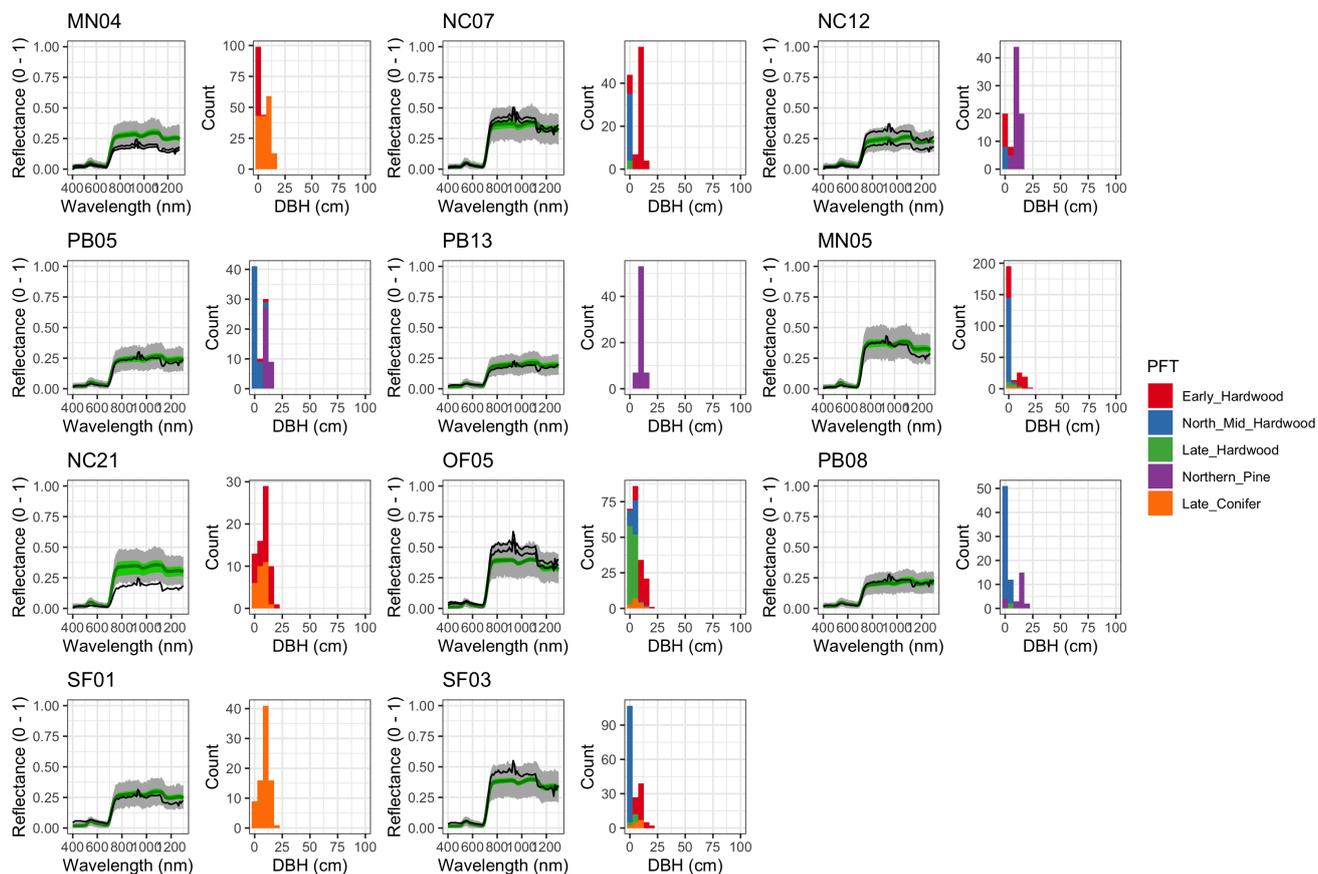
Figure A5. EDR predicted vs. observed spectra and species composition for the first quartile of sites by DBH.
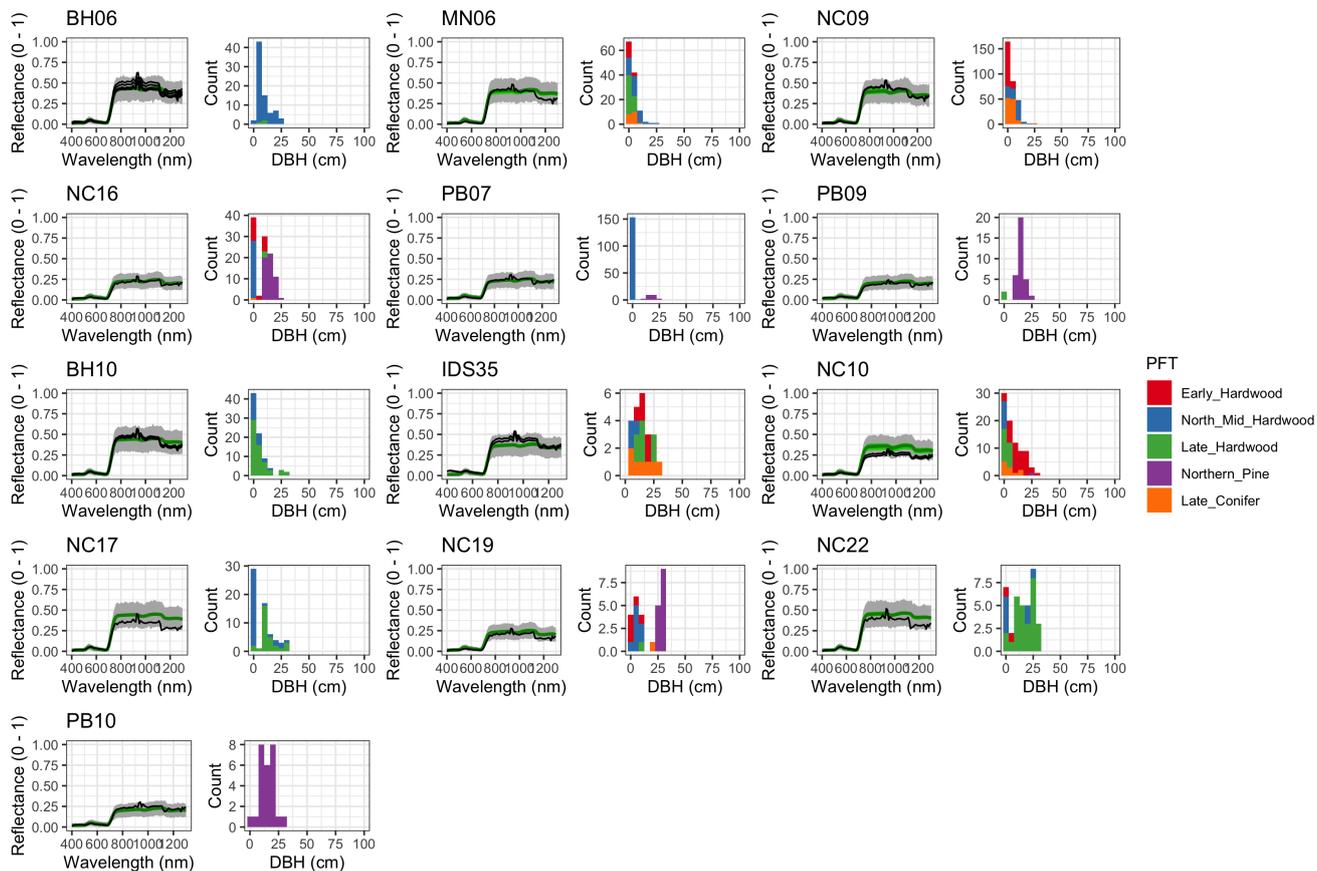
Figure A6. As above, but for the second quartile of sites by DBH.
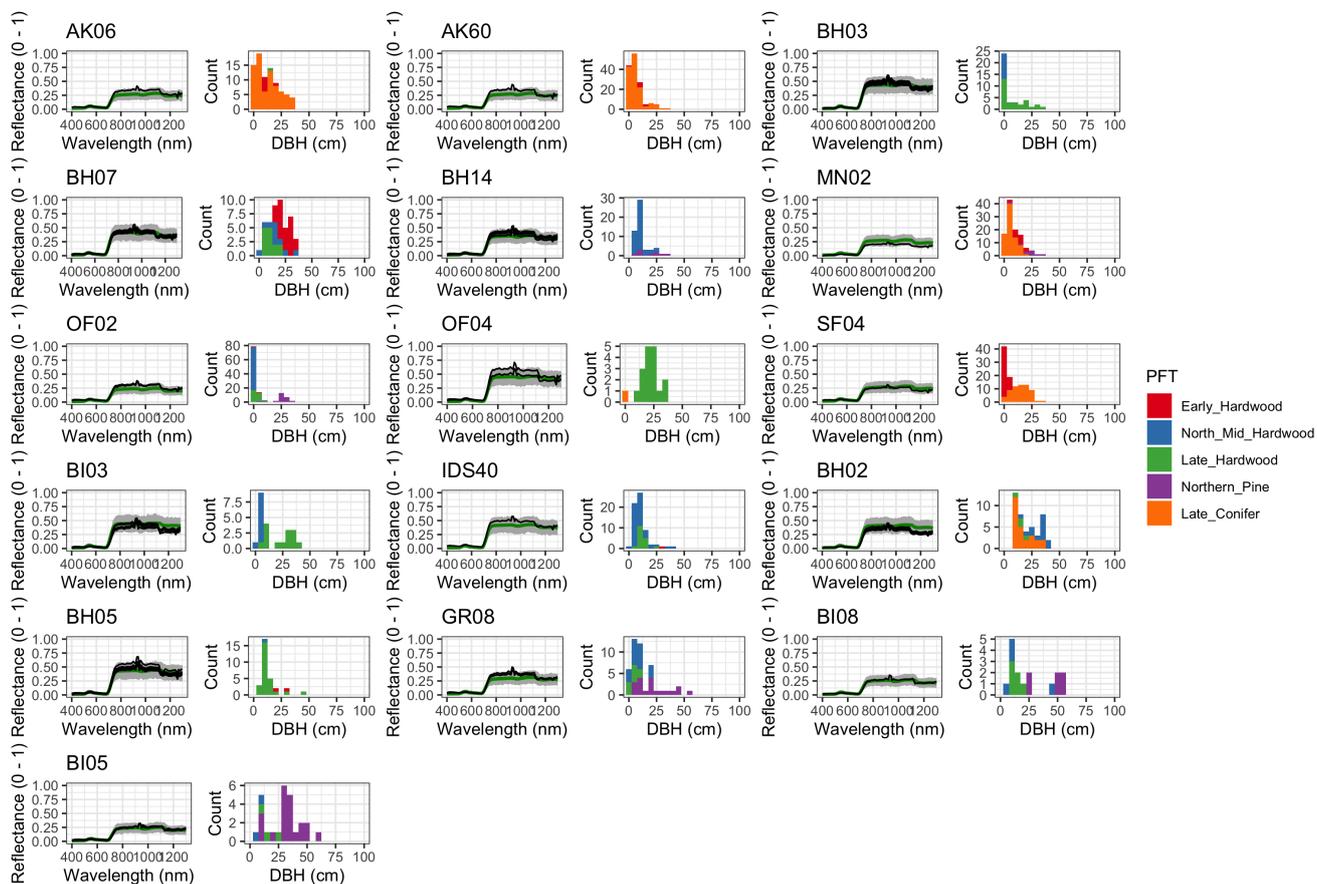
Figure A7. As above, but for the third quartile of sites by DBH.
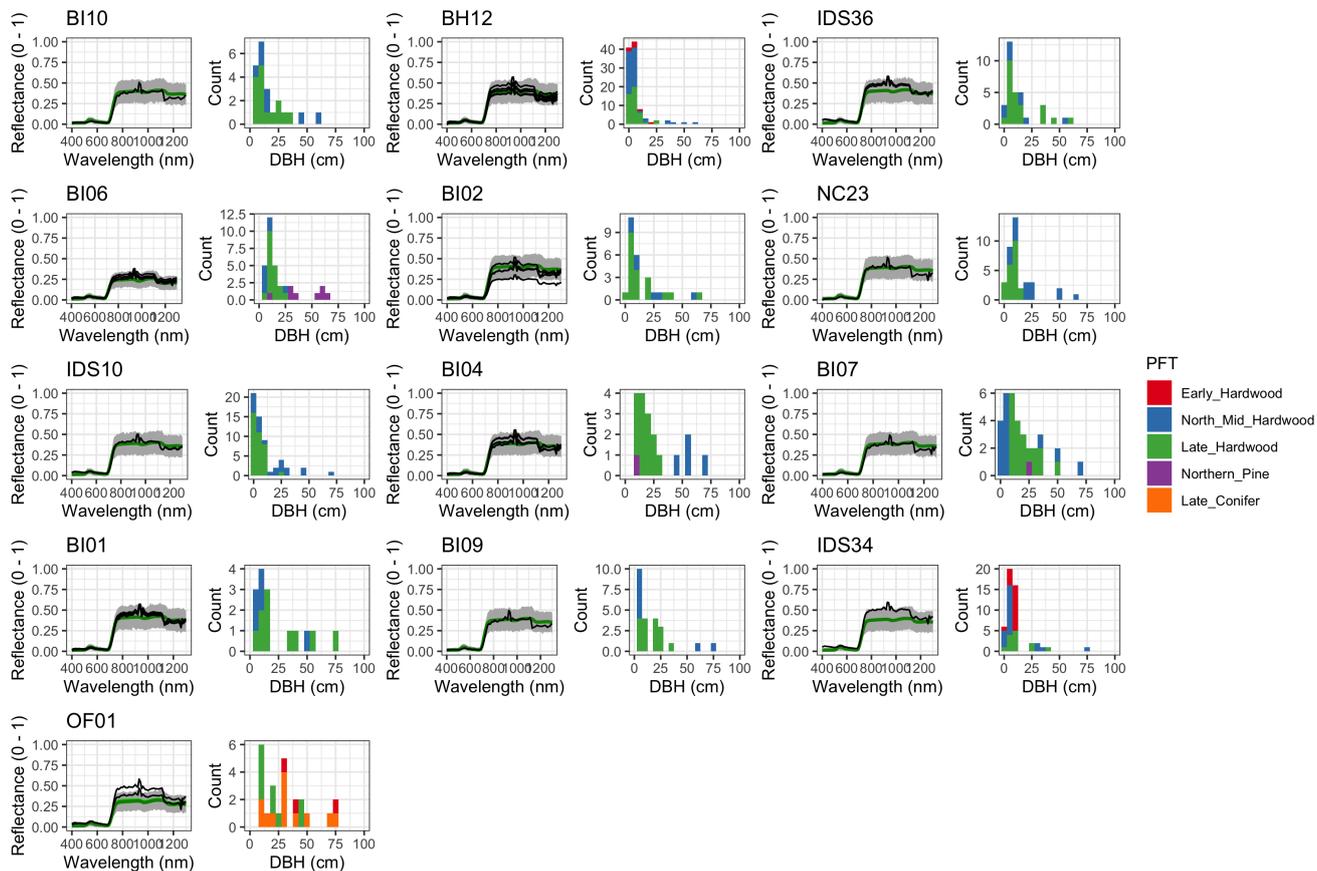
Figure A8. As above, but for the fourth quartile of sites by DBH.
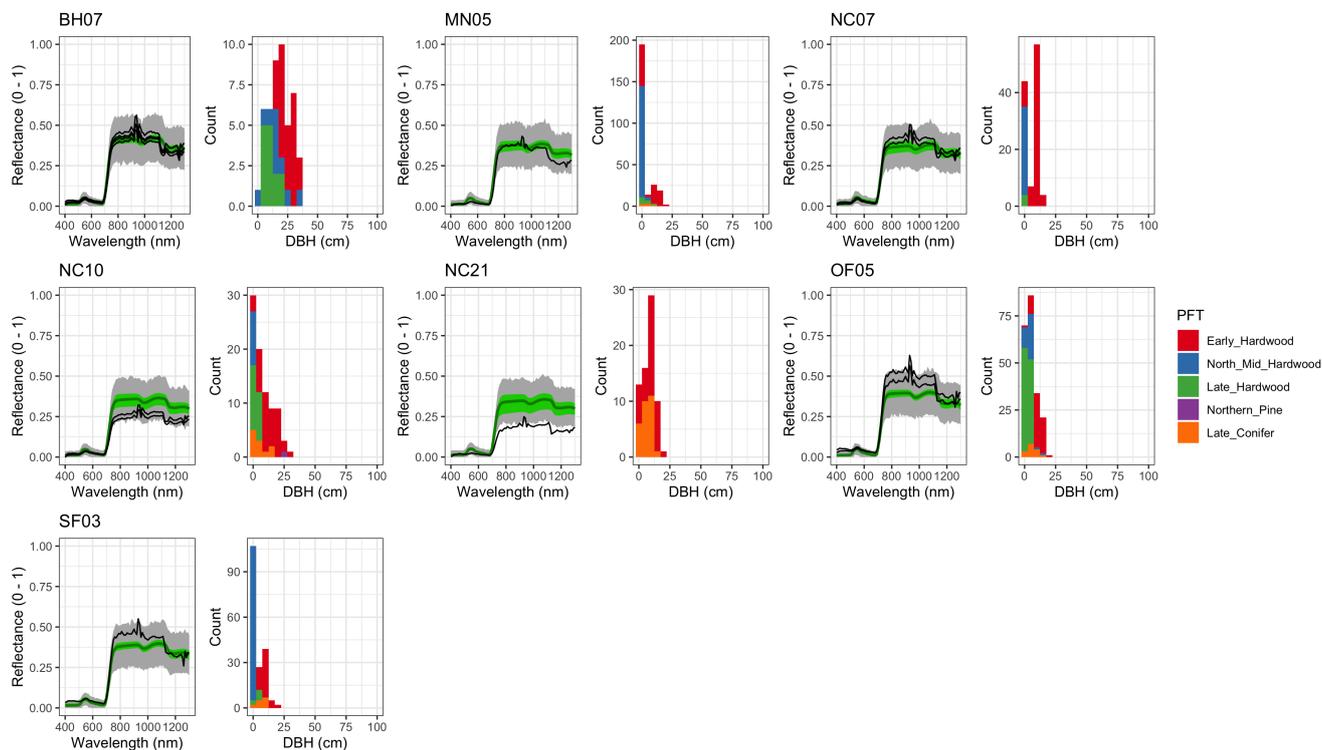
Figure A9. As above, but for sites where Early Hardwood trees had the largest mean DBH.
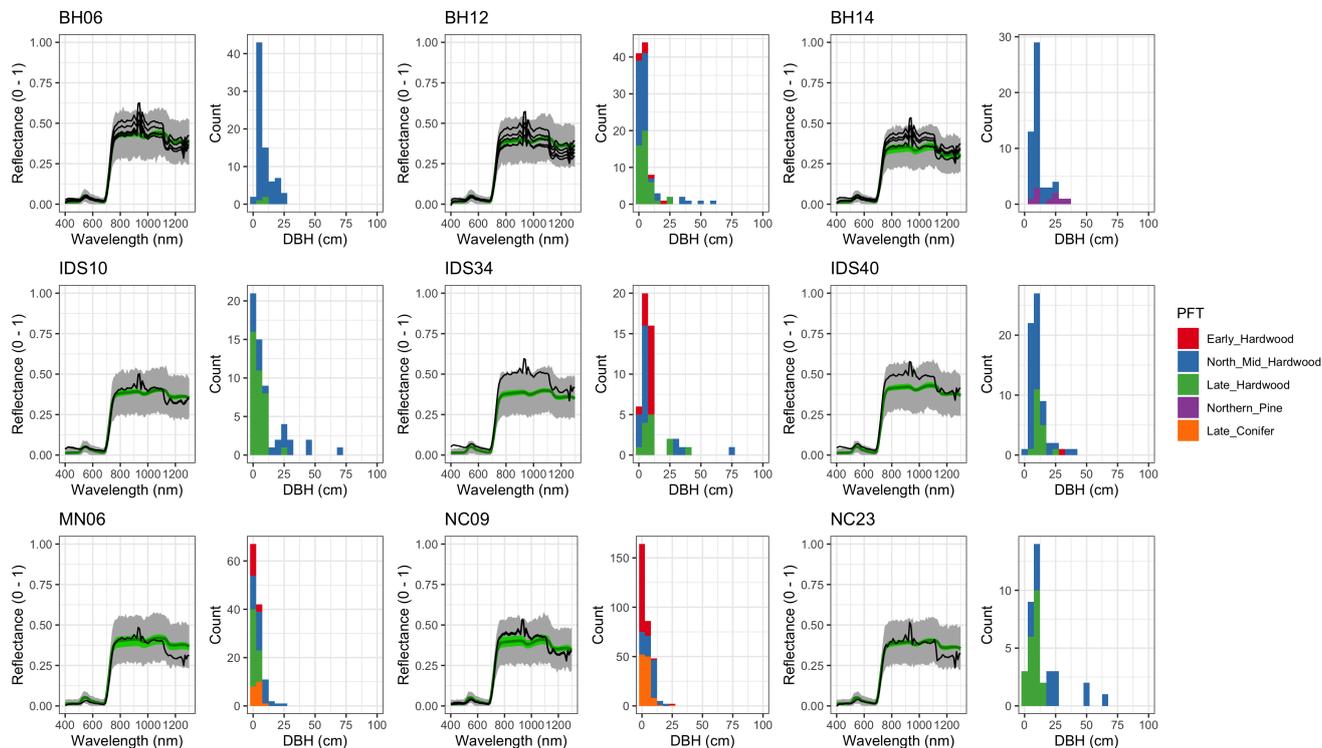
Figure A10. As above, but for sites where Mid Hardwood trees had the largest mean DBH.
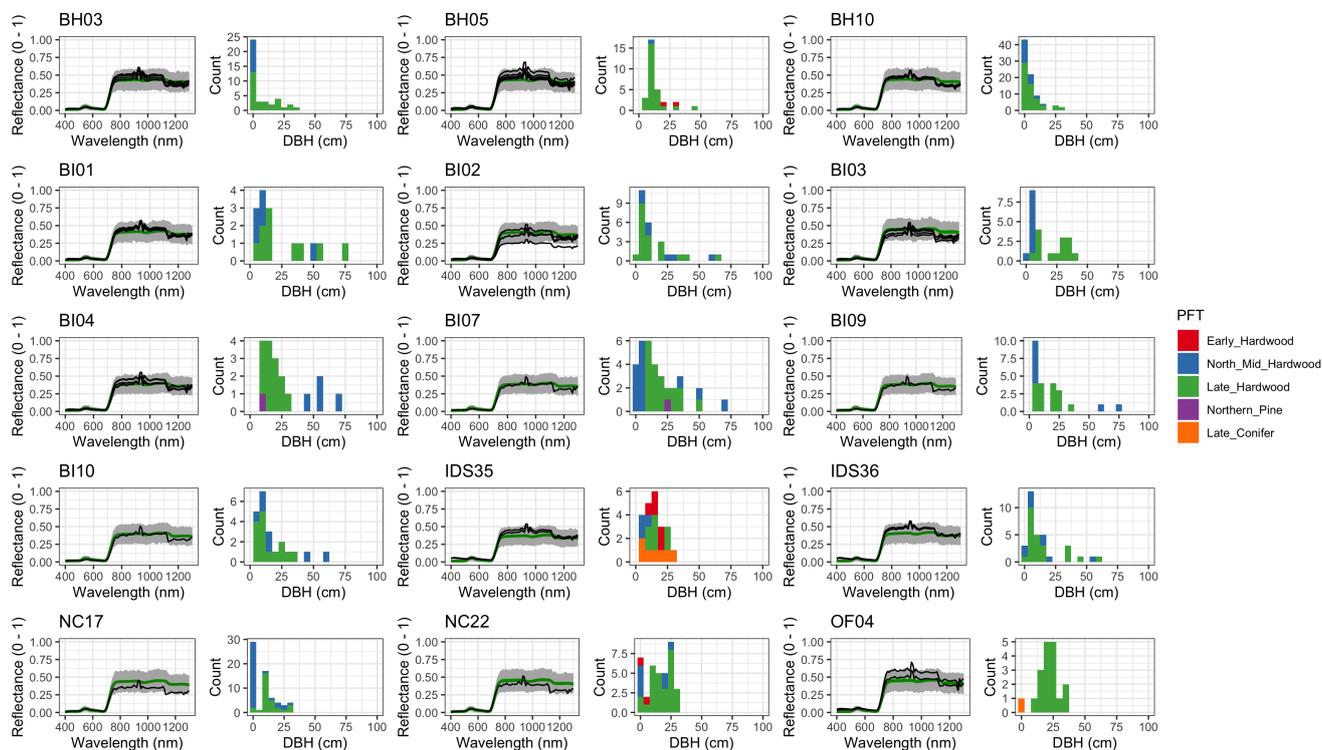
Figure A11. As above, but for sites where Late Hardwood trees had the largest mean DBH.
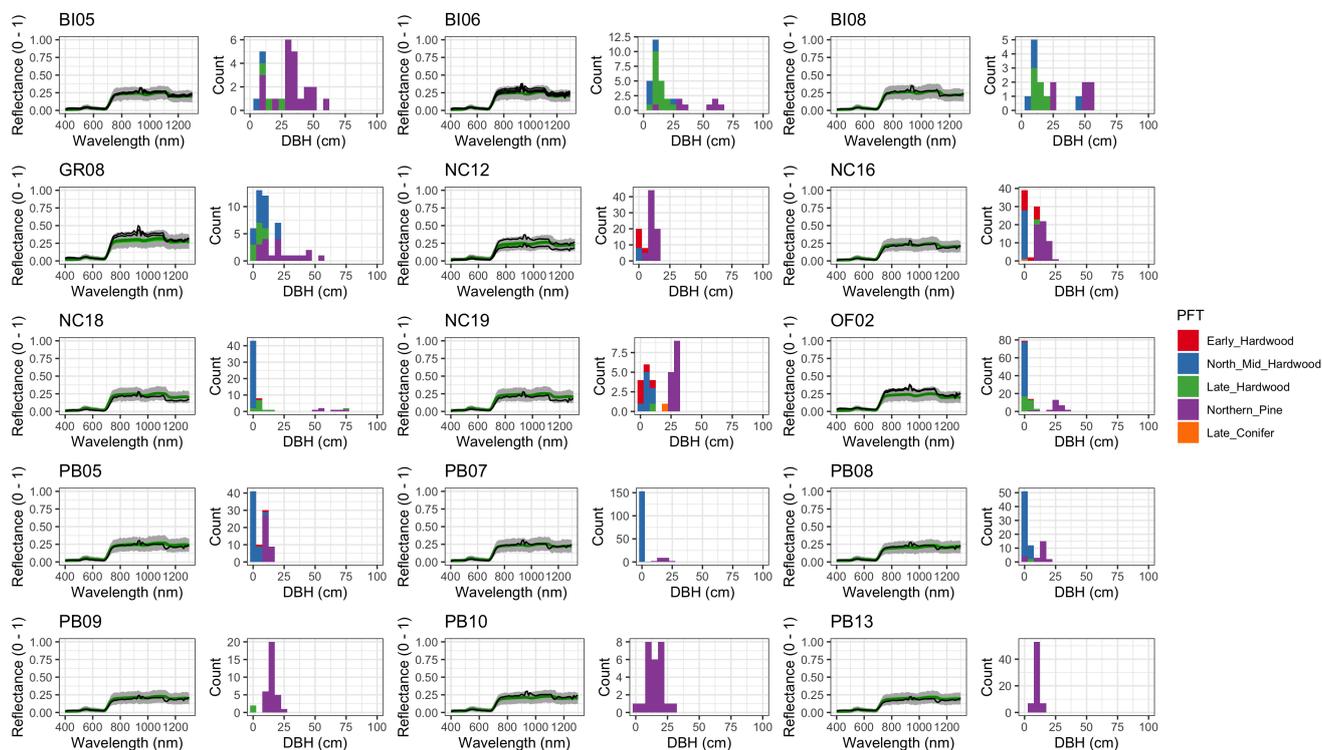
Figure A12. As above, but for sites where Pine trees had the largest mean DBH.
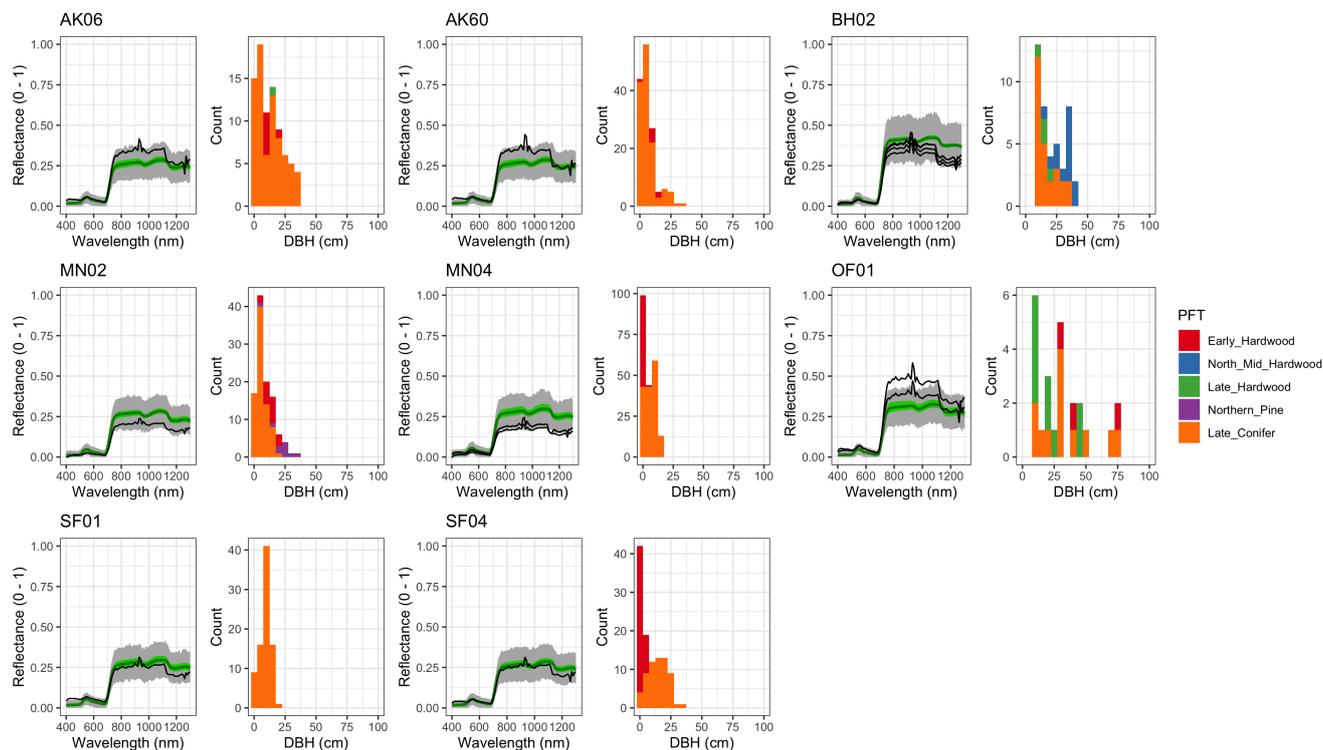
Figure A13. As above, but for sites where Late Conifer trees had the largest mean DBH.

Author contributions. ANS led the analysis and manuscript preparation. MCD and SPS conceived of the original idea, participated in regular

335 discussions about the study with ANS, and provided funding and infrastructure support. IF provided formatted input data on site structure and composition. TV developed the original version of the EDR code. All authors reviewed the manuscript draft and contributed revisions and suggestions.

Competing interests. The authors declare no competing interests.

Acknowledgements. This work was supported financially by NASA awards NNX14AH65G and NNX16AO13H, by NSF Awards 1655095

340 and 1457890, and by NASA's Surface Biology and Geology (SBG) mission study. Cyberinfrastructure for this work was provided by the Boston University Department of Earth and Environment, Brookhaven National Laboratory, Pacific Northwest National Laboratory, and NASA High-End Computing (HEC).

References

Asner, G. P.: Biophysical and Biochemical Sources of Variability in Canopy Reflectance, Remote Sensing of Environment, 64, 234–253, https://doi.org/10.1016/S0034-4257(98)00014-5, 1998.

Baker, I. T., Prihodko, L., Denning, A. S., Goulden, M., Miller, S., and da Rocha, H. R.: Seasonal Drought Stress in the Amazon: Reconciling Models and Observations, Journal of Geophysical Research: Biogeosciences, 113, https://doi.org/10.1029/2007JG000644, 2008.

Best, M. J., Pryor, M., Clark, D. B., Rooney, G. G., Essery, R. L. H., Ménard, C. B., Edwards, J. M., Hendry, M. A., Porson, A., Gedney, N., and al., e.: The Joint UK Land Environment Simulator (JULES), Model Description - Part 1: Energy and Water Fluxes, Geoscientific Model Development, 4, 677–699, https://doi.org/10.5194/gmd-4-677-2011, 2011.

Bonan, G. B.: Forests and Climate Change: Forcings, Feedbacks, and the Climate Benefits of Forests, Science, 320, 1444–1449, https://doi.org/10.1126/science.1155121, 2008.

Combal, B., Baret, F., Weiss, M., Trubuil, A., Macé, D., Pragnère, A., Myneni, R., Knyazikhin, Y., and Wang, L.: Retrieval of Canopy Biophysical Variables from Bidirectional Reflectance: Using Prior Information to Solve the Ill-Posed Inverse Problem, Remote Sensing of Environment, 84, 1–15, https://doi.org/10.1016/S0034-4257(02)00035-4, 2003.

Dickinson, R. E.: Land Surface Processes and Climate—Surface Albedos and Energy Balance, in: Advances in Geophysics, edited by Saltzman, B., vol. 25 of *Theory of ClimateProceedings of a Symposium Commemorating the Two-Hundredth Anniversary of the Academy of Sciences of Lisbon*, pp. 305–353, Elsevier, 1983a.

Dickinson, R. E.: Land Surface Processes and Climate-Surface Albedos and Energy Balance, Advances in Geophysics, 25, 305–353, https://doi.org/10.1016/s0065-2687(08)60176-4, 1983b.

Fensholt, R., Sandholt, I., and Rasmussen, M. S.: Evaluation of MODIS LAI, fAPAR and the Relation between fAPAR and NDVI in a Semi-Arid Environment Using in Situ Measurements, Remote Sensing of Environment, 91, 490–507, https://doi.org/10.1016/j.rse.2004.04.009, 2004.

Feret, J.-B., François, C., Asner, G. P., Gitelson, A. A., Martin, R. E., Bidel, L. P. R., Ustin, S. L., le Maire, G., and Jacquemoud, S.: PROSPECT-4 and 5: Advances in the Leaf Optical Properties Model Separating Photosynthetic Pigments, Remote Sensing of Environment, 112, 3030–3043, https://doi.org/10.1016/j.rse.2008.02.012, 2008.

Fisher, R. A., Koven, C. D., Anderegg, W. R. L., Christoffersen, B. O., Dietze, M. C., Farrior, C. E., Holm, J. A., Hurtt, G. C., Knox, R. G., Lawrence, P. J., Lichstein, J. W., Longo, M., Matheny, A. M., Medvigy, D., Muller-Landau, H. C., Powell, T. L., Serbin, S. P., Sato, H., Shuman, J. K., Smith, B., Trugman, A. T., Viskari, T., Verbeeck, H., Weng, E., Xu, C., Xu, X., Zhang, T., and Moorcroft, P. R.: Vegetation Demographics in Earth System Models: A Review of Progress and Priorities, Global Change Biology, 24, 35–54, https://doi.org/10.1111/gcb.13910, 2018.

Gelman, A. and Rubin, D. B.: Inference from Iterative Simulation Using Multiple Sequences, Statistical Science, 7, 457–472, 1992.

Goudriaan, J.: Crop Micrometeorology: A Simulation Study, Ph.D. thesis, Wageningen University, 1977.

Hartig, F., Minunno, F., and Paul, S.: BayesianTools: General-Purpose MCMC and SMC Samplers and Tools for Bayesian Statistics, https://CRAN.R-project.org/package=BayesianTools, r package version 0.1.7, 2019.

Heinze, C., Eyring, V., Friedlingstein, P., Jones, C., Balkanski, Y., Collins, W., Fichefet, T., Gao, S., Hall, A., Ivanova, D., and al., e.: ESD Reviews: Climate Feedbacks in the Earth System and Prospects for Their Evaluation, Earth System Dynamics, 10, 379–452, https://doi.org/10.5194/esd-10-379-2019, 2019.

Hikosaka, K. and Terashima, I.: A Model of the Acclimation of Photosynthesis in the Leaves of C3 Plants to Sun and Shade with Respect to
Nitrogen Use, Plant, Cell and Environment, 18, 605–618, https://doi.org/10.1111/j.1365-3040.1995.tb00562.x, 1995.

Hogan, R. J., Quaife, T., and Braghiere, R.: Fast Matrix Treatment of 3-D Radiative Transfer in Vegetation Canopies: SPARTACUS-
Vegetation 1.1, Geoscientific Model Development, 11, 339–350, https://doi.org/10.5194/gmd-11-339-2018, 2018.

Huntingford, C., Fisher, R. A., Mercado, L., Booth, B. B., Sitch, S., Harris, P. P., Cox, P. M., Jones, C. D., Betts, R. A., Malhi, Y., Harris,
G. R., Collins, M., and Moorcroft, P.: Towards Quantifying Uncertainty in Predictions of Amazon 'Dieback', Philosophical Transactions
of the Royal Society B: Biological Sciences, 363, 1857–1864, https://doi.org/10.1098/rstb.2007.0028, 2008.

Ivanov, V. Y., Bras, R. L., and Vivoni, E. R.: Vegetation-Hydrology Dynamics in Complex Terrain of Semiarid Areas: 1. A Mechanistic
Approach to Modeling Dynamic Feedbacks, Water Resources Research, 44, https://doi.org/10.1029/2006WR005588, 2008.

Jacquemoud, S., Verhoef, W., Baret, F., Bacour, C., Zarco-Tejada, P. J., Asner, G. P., François, C., and Ustin, S. L.: PROSPECT +
SAIL Models: A Review of Use for Vegetation Characterization, Remote Sensing of Environment, 113, Supplement 1, S56–S66,
https://doi.org/10.1016/j.rse.2008.01.026, 2009.

Jenkins, J. C., Chojnacky, D. C., Heath, L. S., and Birdsey, R. A.: National-Scale Biomass Estimators for United States Tree Species, Forest
Science, 49, 12–35, 2003.

Jenkins, J. C., Chojnacky, D. C., Heath, L. S., and Birdsey, R. A.: Comprehensive Database of Diameter-Based Biomass Regressions for
North American Tree Species, Tech. Rep. NE-GTR-319, U.S. Department of Agriculture, Forest Service, Northeastern Research Station,
Newtown Square, PA, https://doi.org/10.2737/NE-GTR-319, 2004.

Jetz, W., Cavender-Bares, J., Pavlick, R., Schimel, D., Davis, F. W., Asner, G. P., Guralnick, R., Kattge, J., Latimer, A. M., Moorcroft, P.,
Schaepman, M. E., Schildhauer, M. P., Schneider, F. D., Schrodt, F., Stahl, U., and Ustin, S. L.: Monitoring Plant Functional Diversity
from Space, Nature Plants, p. 16039, https://doi.org/10.1038/nplants.2016.39, 2016.

Keenan, T. F. and Niinemets, Ü.: Global Leaf Trait Estimates Biased Due to Plasticity in the Shade, Nature Plants, 3, 16 201,
https://doi.org/10.1038/nplants.2016.201, 2016.

Kennedy, R. E., Andréfouët, S., Cohen, W. B., Gómez, C., Griffiths, P., Hais, M., Healey, S. P., Helmer, E. H., Hostert, P., Lyons, M. B., Meigs,
G. W., Pflugmacher, D., Phinn, S. R., Powell, S. L., Scarth, P., Sen, S., Schroeder, T. A., Schneider, A., Sonnenschein, R., Vogelmann,
J. E., Wulder, M. A., and Zhu, Z.: Bringing an Ecological View of Change to Landsat-Based Remote Sensing, Frontiers in Ecology and
the Environment, 12, 339–346, https://doi.org/10.1890/130066, 2014.

Knorr, W. and Lakshmi, V.: Assimilation of FAPAR and Surface Temperature into a Land Surface and Vegetation Model, in: Land
Surface Hydrology, Meteorology, and Climate: Observations and Modeling, pp. 177–200, American Geophysical Union (AGU),
https://doi.org/10.1029/WS003p0177, 2001.

Knorr, W., Kaminski, T., Scholze, M., Gobron, N., Pinty, B., Giering, R., and Mathieu, P.-P.: Carbon Cycle Data Assimilation with a Generic
Phenology Model, Journal of Geophysical Research: Biogeosciences, 115, https://doi.org/10.1029/2009JG001119, 2010.

Koven, C. D., Knox, R. G., Fisher, R. A., Chambers, J. Q., Christoffersen, B. O., Davies, S. J., Detto, M., Dietze, M. C., Faybishenko, B.,
Holm, J., Huang, M., Kovenock, M., Kueppers, L. M., Lemieux, G., Massoud, E., McDowell, N. G., Muller-Landau, H. C., Needham,
J. F., Norby, R. J., Powell, T., Rogers, A., Serbin, S. P., Shuman, J. K., Swann, A. L. S., Varadharajan, C., Walker, A. P., Wright, S. J., and
Xu, C.: Benchmarking and Parameter Sensitivity of Physiological and Vegetation Dynamics Using the Functionally Assembled Terrestrial
Ecosystem Simulator (FATES) at Barro Colorado Island, Panama, Biogeosciences, 17, 3017–3044, https://doi.org/10.5194/bg-17-3017-
2020, 2020.

Lewis, P. and Disney, M.: Spectral Invariants and Scattering across Multiple Scales from Within-Leaf to Canopy, Remote Sensing of Environment, 109, 196–206, https://doi.org/10.1016/j.rse.2006.12.015, 2007.

Liu, Y., Xiao, J., Ju, W., Zhu, G., Wu, X., Fan, W., Li, D., and Zhou, Y.: Satellite-Derived LAI Products Exhibit Large Discrepancies and Can Lead to Substantial Uncertainty in Simulated Carbon and Water Fluxes, Remote Sensing of Environment, 206, 174–188,
420   https://doi.org/10.1016/j.rse.2017.12.024, 2018.

Loew, A., van Bodegom, P. M., Widlowski, J.-L., Otto, J., Quaife, T., Pinty, B., and Raddatz, T.: Do We (Need to) Care about Canopy Radiation Schemes in DGVMs? Caveats and Potential Impacts, Biogeosciences, 11, 1873–1897, https://doi.org/10.5194/bg-11-1873-2014, 2014.

Longo, M., Knox, R. G., Medvigy, D. M., Levine, N. M., Dietze, M. C., Kim, Y., Swann, A. L. S., Zhang, K., Rollinson, C. R., Bras, R. L., and
425   al., e.: The Biophysics, Ecology, and Biogeochemistry of Functionally Diverse, Vertically- and Horizontally-Heterogeneous Ecosystems: The Ecosystem Demography Model, Version 2.2 - Part 1: Model Description, Geoscientific Model Development Discussions, pp. 1–53, https://doi.org/10.5194/gmd-2019-45, 2019a.

Longo, M., Knox, R. G., Medvigy, D. M., Levine, N. M., Dietze, M. C., Kim, Y., Swann, A. L. S., Zhang, K., Rollinson, C. R., Bras, R. L., Wofsy, S. C., and Moorcroft, P. R.: The Biophysics, Ecology, and Biogeochemistry of Functionally Diverse, Vertically and Hori-
430   zontally Heterogeneous Ecosystems: The Ecosystem Demography Model, Version 2.2 – Part 1: Model Description, Geoscientific Model Development, 12, 4309–4346, https://doi.org/10.5194/gmd-12-4309-2019, 2019b.

MacBean, N., Maignan, F., Bacour, C., Lewis, P., Peylin, P., Guanter, L., Köhler, P., Gómez-Dans, J., and Disney, M.: Strong Constraint on Modelled Global Carbon Uptake Using Solar-Induced Chlorophyll Fluorescence Data, Scientific Reports, 8, 1973, https://doi.org/10.1038/s41598-018-20024-w, 2018.

435 Maignan, F., Bréon, F. M., and Lacaze, R.: Bidirectional Reflectance of Earth Targets: Evaluation of Analytical Models Using a Large Set of Spaceborne Measurements with Emphasis on the Hot Spot, Remote Sensing of Environment, 90, 210–220, https://doi.org/10.1016/j.rse.2003.12.006, 2004.

McMahon, S. M., Harrison, S. P., Armbruster, W. S., Bartlein, P. J., Beale, C. M., Edwards, M. E., Kattge, J., Midgley, G., Morin, X., and Prentice, I. C.: Improving Assessment and Modelling of Climate Change Impacts on Global Terrestrial Biodiversity, Trends in Ecology &
440   Evolution, 26, 249–259, https://doi.org/10.1016/j.tree.2011.02.012, 2011.

Medvigy, D., Wofsy, S. C., Munger, J. W., Hollinger, D. Y., and Moorcroft, P. R.: Mechanistic Scaling of Ecosystem Function and Dynamics in Space and Time: Ecosystem Demography Model Version 2, Journal of Geophysical Research: Biogeosciences, 114, G01 002, https://doi.org/10.1029/2008JG000812, 2009.

Moorcroft, P. R., Hurtt, G. C., and Pacala, S. W.: A Method for Scaling Vegetation Dynamics: The Ecosystem Demography Model (ED),
445   Ecological Monographs, 71, 557–586, https://doi.org/10.1890/0012-9615(2001)071[0557:amfsvd]2.0.co;2, 2001.

Myneni, R. and Williams, D.: On the Relationship between FAPAR and NDVI, Remote Sensing of Environment, 49, 200–211, https://doi.org/10.1016/0034-4257(94)90016-7, 1994.

Niinemets, Ü.: Within-Canopy Variations in Functional Leaf Traits: Structural, Chemical and Ecological Controls and Diversity of Responses, in: Canopy Photosynthesis: From Basics to Applications, edited by Hikosaka, K., Niinemets, Ü., and Anten, N. P. R., no. 42 in
450   Advances in Photosynthesis and Respiration, pp. 101–141, [object Object], https://doi.org/10.1007/978-94-017-7291-4_4, 2016.

Niu, G.-Y., Yang, Z.-L., Mitchell, K. E., Chen, F., Ek, M. B., Barlage, M., Kumar, A., Manning, K., Niyogi, D., Rosero, E., Tewari, M., and Xia, Y.: The Community Noah Land Surface Model with Multiparameterization Options (Noah-MP): 1. Model Description and Evaluation with Local-Scale Measurements, Journal of Geophysical Research: Atmospheres, 116, https://doi.org/10.1029/2010JD015139, 2011.

Nouvellon, Y., Moran, M. S., Seen, D. L., Bryant, R., Rambal, S., Ni, W., Bégué, A., Chehbouni, A., Emmerich, W. E., Heilman, P., and
    Qi, J.: Coupling a Grassland Ecosystem Model with Landsat Imagery for a 10-Year Simulation of Carbon and Water Budgets, Remote
    Sensing of Environment, 78, 131–149, https://doi.org/10.1016/S0034-4257(01)00255-3, 2001.

Oleson, K. W., Lawrence, D. M., Bonan, G. B., Drewniak, B., Huang, M., Koven, C. D., Levis, S., Li, F., Riley, W. J., Subin, Z. M., Swenson,
    S. C., Thornton, P., Bozbiyik, A., Fisher, R., Heald, C. L., Kluzek, E., Lamarque, J.-F., Lawrence, P. J., Leung, R., Lipscom, W., Muszala,
    S., Ricciuto, D. M., Sacks, W., Sun, Y., Tang, J., and Zong-Liang, Y.: Technical Description of Version 4.5 of the Community Land Model
    (CLM), Tech. Rep. NCAR/TN-503+STR, NCAR Earth System Laboratory Climate and Global Dynamics Division, 2013.

Pacala, S. W. and Deutschman, D. H.: Details That Matter: The Spatial Distribution of Individual Trees Maintains Forest Ecosystem Function,
    Oikos, 74, 357, https://doi.org/10.2307/3545980, 1995.

Pasquarella, V. J., Holden, C. E., Kaufman, L., and Woodcock, C. E.: From Imagery to Ecology: Leveraging Time Series of All Available
    Landsat Observations to Map and Monitor Ecosystem State and Dynamics, Remote Sensing in Ecology and Conservation, pp. n/a–n/a,
    https://doi.org/10.1002/rse2.24, 2016.

Peylin, P., Bacour, C., MacBean, N., Leonard, S., Rayner, P., Kuppel, S., Koffi, E., Kane, A., Maignan, F., Chevallier, F., Ciais, P., and Prunet,
    P.: A New Stepwise Carbon Cycle Data Assimilation System Using Multiple Data Streams to Constrain the Simulated Land Surface
    Carbon Cycle, Geoscientific Model Development, 9, 3321–3346, https://doi.org/10.5194/gmd-9-3321-2016, 2016.

Pinty, B., Gobron, N., Widlowski, J.-L., Lavergne, T., and Verstraete, M. M.: Synergy between 1-D and 3-D Radiation Transfer Models
    to Retrieve Vegetation Canopy Properties from Remote Sensing Data, Journal of Geophysical Research: Atmospheres, 109, D21 205,
    https://doi.org/10.1029/2004JD005214, 2004.

Quaife, T., Lewis, P., De Kauwe, M., Williams, M., Law, B. E., Disney, M., and Bowyer, P.: Assimilating Canopy Re-
    flectance Data into an Ecosystem Model with an Ensemble Kalman Filter, Remote Sensing of Environment, 112, 1347–1364,
    https://doi.org/10.1016/j.rse.2007.05.020, 2008.

Robakowski, P., Wyka, T., Samardakiewicz, S., and Kierzkowski, D.: Growth, Photosynthesis, and Needle Structure of Silver Fir (Abies Alba
    Mill.) Seedlings under Different Canopies, Forest Ecology and Management, 201, 211–227, https://doi.org/10.1016/j.foreco.2004.06.029,
    2004.

Running, S. W., Nemani, R. R., Heinsch, F. A., Zhao, M., Reeves, M., and Hashimoto, H.: A Continuous Satellite-Derived Measure of Global
    Terrestrial Primary Production, BioScience, 54, 547–560, https://doi.org/10.1641/0006-3568(2004)054[0547:ACSMOG]2.0.CO;2, 2004.

Schaepman-Strub, G., Schaepman, M. E., Painter, T. H., Dangel, S., and Martonchik, J. V.: Reflectance Quantities in Optical Remote Sens-
    ing—Definitions and Case Studies, Remote Sensing of Environment, 103, 27–42, https://doi.org/10.1016/j.rse.2006.03.002, 2006.

Schimel, D., Pavlick, R., Fisher, J. B., Asner, G. P., Saatchi, S., Townsend, P., Miller, C., Frankenberg, C., Hibbard, K., and Cox, P.: Observing
    Terrestrial Ecosystems and the Carbon Cycle from Space, Global Change Biology, 21, 1762–1776, https://doi.org/10.1111/gcb.12822,
    2015.

Schürmann, G. J., Kaminski, T., Köstler, C., Carvalhais, N., Voßbeck, M., Kattge, J., Giering, R., Rödenbeck, C., Heimann, M., and Zaehle,
    S.: Constraining a Land-Surface Model with Multiple Observations by Application of the MPI-Carbon Cycle Data Assimilation System
    V1.0, Geoscientific Model Development, 9, 2999–3026, https://doi.org/10.5194/gmd-9-2999-2016, 2016.

Sellers, P. J.: Canopy Reflectance, Photosynthesis and Transpiration, International Journal of Remote Sensing, 6, 1335–1372,
    https://doi.org/10.1080/01431168508948283, 1985.

Shiklomanov, A. N.: Improving Ecological Forecasts Using Model and Data Constraints, Ph.D. thesis, Boston University, 2018.

Shiklomanov, A. N., Dietze, M. C., Viskari, T., Townsend, P. A., and Serbin, S. P.: Quantifying the Influences of Spectral Resolution on Uncertainty in Leaf Trait Estimates through a Bayesian Approach to RTM Inversion, Remote Sensing of Environment, 183, 226–238, https://doi.org/10.1016/j.rse.2016.05.023, 2016.

Shiklomanov, A. N., Cowdery, E. M., Bahn, M., Byun, C., Jansen, S., Kramer, K., Minden, V., Niinemets, Ü., Onoda, Y., Soudzilovskaia, N. A., and Dietze, M. C.: Does the Leaf Economic Spectrum Hold within Plant Functional Types? A Bayesian Multivariate Trait Meta-analysis, Ecological Applications, 30, https://doi.org/10.1002/eap.2064, 2020.

Swann, A. L., Fung, I. Y., Levis, S., Bonan, G. B., and Doney, S. C.: Changes in Arctic Vegetation Amplify High-Latitude Warming through the Greenhouse Effect, Proceedings of the National Academy of Sciences, 107, 1295–1300, https://doi.org/10.1073/pnas.0913846107, 2010.

Swann, A. L. S., Fung, I. Y., and Chiang, J. C. H.: Mid-Latitude Afforestation Shifts General Circulation and Tropical Precipitation, Proceedings of the National Academy of Sciences, 109, 712–716, https://doi.org/10.1073/pnas.1116706108, 2012.

ter Braak, C. J. F. and Vrugt, J. A.: Differential Evolution Markov Chain with Snooker Updater and Fewer Chains, Statistics and Computing, 18, 435–446, https://doi.org/10.1007/s11222-008-9104-9, 2008.

Verhoef, W.: Light Scattering by Leaf Layers with Application to Canopy Reflectance Modeling: The SAIL Model, Remote Sensing of Environment, 16, 125–141, https://doi.org/10.1016/0034-4257(84)90057-9, 1984.

Verhoef, W. and Bach, H.: Coupled Soil–Leaf-Canopy and Atmosphere Radiative Transfer Modeling to Simulate Hyperspectral Multi-Angular Surface Reflectance and TOA Radiance Data, Remote Sensing of Environment, 109, 166–182, https://doi.org/10.1016/j.rse.2006.12.013, 2007.

Viskari, T., Hardiman, B., Desai, A. R., and Dietze, M. C.: Model-Data Assimilation of Multiple Phenological Observations to Constrain and Predict Leaf Area Index, Ecological Applications, 25, 546–558, https://doi.org/10.1890/14-0497.1, 2015.

Viskari, T., Shiklomanov, A., Dietze, M. C., and Serbin, S. P.: The Influence of Canopy Radiation Parameter Uncertainty on Model Projections of Terrestrial Carbon and Energy Cycling, PLOS ONE, 14, e0216 512, https://doi.org/10.1371/journal.pone.0216512, 2019.

Widlowski, J.-L., Taberner, M., Pinty, B., Bruniquel-Pinel, V., Disney, M., Fernandes, R., Gastellu-Etchegorry, J.-P., Gobron, N., Kuusk, A., Lavergne, T., Leblanc, S., Lewis, P. E., Martin, E., Mõttus, M., North, P. R. J., Qin, W., Robustelli, M., Rochdi, N., Ruiloba, R., Soler, C., Thompson, R., Verhoef, W., Verstraete, M. M., and Xie, D.: Third Radiation Transfer Model Intercomparison (RAMI) Exercise: Documenting Progress in Canopy Reflectance Models, Journal of Geophysical Research: Atmospheres, 112, D09 111, https://doi.org/10.1029/2006JD007821, 2007.

Widlowski, J.-L., Mio, C., Disney, M., Adams, J., Andredakis, I., Atzberger, C., Brennan, J., Busetto, L., Chelle, M., Ceccherini, G., Colombo, R., Côté, J.-F., Eenmäe, A., Essery, R., Gastellu-Etchegorry, J.-P., Gobron, N., Grau, E., Haverd, V., Homolová, L., Huang, H., Hunt, L., Kobayashi, H., Koetz, B., Kuusk, A., Kuusk, J., Lang, M., Lewis, P. E., Lovell, J. L., Malenovský, Z., Meroni, M., Morsdorf, F., Mõttus, M., Ni-Meister, W., Pinty, B., Rautiainen, M., Schlerf, M., Somers, B., Stuckens, J., Verstraete, M. M., Yang, W., Zhao, F., and Zenone, T.: The Fourth Phase of the Radiative Transfer Model Intercomparison (RAMI) Exercise: Actual Canopy Scenarios and Conformity Testing, Remote Sensing of Environment, 169, 418–437, https://doi.org/10.1016/j.rse.2015.08.016, 2015.

Yuan, H., Dai, Y., Dickinson, R. E., Pinty, B., Shangguan, W., Zhang, S., Wang, L., and Zhu, S.: Reexamination and Further Development of Two-Stream Canopy Radiative Transfer Models for Global Land Modeling, Journal of Advances in Modeling Earth Systems, 9, 113–129, https://doi.org/10.1002/2016MS000773, 2017.

Zhang, Q., Yao, T., Huemmrich, K. F., Middleton, E. M., Lyapustin, A., and Wang, Y.: Evaluating Impacts of Snow, Surface Water, Soil and Vegetation on Empirical Vegetation and Snow Indices for the Utqiaġvik Tundra Ecosystem in Alaska with the LVS3 Model, Remote Sensing of Environment, 240, 111 677, https://doi.org/10.1016/j.rse.2020.111677, 2020.

530 Zobitz, J., Moore, D. J., Quaife, T., Braswell, B. H., Bergeson, A., Anthony, J. A., and Monson, R. K.: Joint Data Assimilation of Satellite Reflectance and Net Ecosystem Exchange Data Constrains Ecosystem Carbon Fluxes at a High-Elevation Subalpine Forest, Agricultural and Forest Meteorology, 195-196, 73–88, https://doi.org/10.1016/j.agrformet.2014.04.011, 2014.